

POLITECNICO DI TORINO

Collegio di Ingegneria Energetica e Nucleare

**Corso di Laurea Magistrale
in Ingegneria Energetica e Nucleare**

Tesi di Laurea Magistrale

**Development of a dynamic Modelica model of a helium
refrigerator for the cooling of superconducting magnets in
nuclear fusion reactors**



Relatore

Dr. Roberto Bonifetto

Candidato

Pietro Gaiotti

Marzo 2021

Table of Contents

Abstract.....	1
List of symbols and acronyms.....	2
1. Introduction.....	4
1.1. Context: the nuclear fusion reactors.....	4
1.2. Needs for refrigeration in nuclear fusion	8
1.3. Existing fusion experiments and refrigerators	11
1.4. Existing refrigerator models and needs for modelling.....	11
1.5. Aim of the thesis.....	14
1.6. The Modelica language.....	14
2. Description of the Naka refrigerator.....	15
2.1. The naka CSMC facility.....	15
2.2. Layout of the refrigerator	15
2.3. Typical operational transients.....	17
3. Refrigerator model.....	18
3.1. General modelling assumptions.....	24
3.2. Description of the components.....	24
3.2.1. Cold compressor	25
3.2.2. Warm compressor	26
3.2.3. Turbo-expanders	27
3.2.4. Joule-Thomson valves.....	28
3.2.5. SHe Helium Bath.....	28
3.2.6. Heat exchangers	29
4. Simulation setup.....	43
4.1. Pulsed heat source.....	43
4.2. Progressive closure of JT3	44
4.3. CC partial LOFA	44
5. Results	45

6. Conclusions and perspectives.....	50
Bibliography.....	51

Abstract

Magnetically-confined plasmas are currently the most promising technological solution to achieve the target of producing electricity from nuclear fusion reactions. Several experimental reactors, mostly featuring the tokamak configuration, are being operated and designed around the world to address and solve the remaining open issues. The magnetic confinement relies on huge magnetic fields, produced by means of electromagnets, usually wound using superconducting cables. The latter show their superconducting properties only at low (high temperature superconductors) or very low (low temperature superconductors) temperature, so that they must be cooled down to the liquid nitrogen or liquid He temperature, respectively. Such a cryogenic power is provided by a refrigerator, whose technological complexity and cost are a significant fraction of those of the entire machine. For these reasons, a suitable dimensioning and safe operation of the refrigerator is required and can be supported by adequate and reliable models. The latter, however, are currently limited to static or simplified dynamic models used for the industrial dimensioning of the refrigerators.

A new dynamic model of such a refrigerator is developed in this work, based on the object-oriented Modelica programming language. The (5 kW @ 4.5 K) He refrigerator of the ITER Central Solenoid Model Coil (CSMC), installed at the National Institutes for Quantum and Radiological Science and Technology, Naka (Japan), is chosen as reference for the model development, being its thermodynamic cycle fully representative of the refrigerators operating in many existing superconducting magnet facilities as well as in different existing and future tokamaks. Among them, also the Italian Divertor Tokamak Test facility (DTT), currently under construction at ENEA Frascati research center, will be equipped with a He refrigerator for the cooling of its superconducting magnet system.

The model of each component of the refrigerator described in the paper, developed on the basis of the CSMC design data, is independently tested and then added to the “CryoModelica” library, which is also used by the 4C code for the analysis of thermal-hydraulic transients in SC magnets.

The new refrigerator model is tested both in steady-state conditions, where a constant heat source is applied to the system, and in transient mode, where a time varying heat source is instead connected to the refrigerator. The preliminary results are shown to be coherent to what expected from the operation of the real plant in both operation-modes. The model developed here is ready for the implementation of all the necessary controls, needed for the prediction of the refrigerator operation in support of the design of its automatic control strategies.

Keywords: nuclear fusion, superconducting magnets, He refrigerator, thermal-hydraulic modelling, dynamic model.

List of symbols and acronyms

<u>Acronyms</u>	
4C – Cryogenic Circuit Conductor and Coil code	ITER – International Thermonuclear Experimental Reactor
AC – Alternate Current	JT – Joule-Thomson
BC – Boundary Condition	JT-60SA – Japan Tokamak 60 Super Advanced
C – Compressor	KSTAR – Korea Superconducting Tokamak Advanced Research
CB – Cold Box	LHD – Large Helical Device
CC – Cold Compressor	LHe – Liquid Helium
CD – CoolDown	LN ₂ – Liquid N ₂
CEA – Commissariat à l’Energie Atomique et aux énergies alternatives	LP – Low Pressure
CG – Compressor Group	LTS – Low Temperature Superconductors
CICC – Cable In Conduit Conductors	N ₂ – Nitrogen
CS – Central Solenoid	NIFS – National Institute for Fusion Science
CSMC – Central Solenoid Model Coil	NIST – National Institute of Standards and Technology
D – Deuterium	OP – Operating Point
DEMO – Demonstration power plant	PC – Post-Cooled
DTT – Italian Divertor Tokamak Test facility	PF – Poloidal Field
EAST – Experimental Advanced Superconducting Tokamak	PR – Pressure Ratio
FS – Flow Sensor	PS – Pressure Sensor
GHe – Gaseous He	QST – National Institutes for Quantum and Radiological Science and Technology
He – Helium	SC – Superconducting
HeBath = Supercritical Helium Bath	SHe – Supercritical Helium
HELIOS – Helium Loop for hIgh LOads Smoothing	SST – Steady state Superconducting Tokamak
HP – High Pressure	T – Tritium
HTC – Heat Transfer Coefficient	TE – Turbo Expander
HTS – High Temperature Superconductors	TF – Toroidal Field
HX – Heat eXchanger	TH – Thermal-Hydraulic
IPP – Institute for Plasma Physics	TS – Temperature Sensor
IC – Inter-Cooled	UA – Global Heat Transfer Coefficient
	US – United States

Symbols

A – area

b – plate spacing

c – fin pitch

C_v – valve flow coefficient

dm/dt or m – mass flow rate

L - height of the HX

n - number of pipes

N_p - the number of pumps in parallel

p – pressure

Q_{loss} - heat loss of a single pump

S – surface

T – temperature

t – time

V - volume

v - width of the HX

W – compression power

w - depth of the HX

W_{single} - power consumption of a single pump

Greek

β - calibration parameter

Δ – difference

δ – thickness

η – efficiency

ρ – density

1. Introduction

1.1. Context: the nuclear fusion reactors

Energy plays an ever-growing role in almost every aspect of human life. Its applications spread widely in numerous fields like industrial, transport, residential, medicine, research, social life. Moreover, the last two centuries have witnessed an impressive technological development and a parallel exponential growth of the amount of the global energy consumed. Over the last 200 years the world energy consumption has increased by something like 3000% (see **Figure 1**). Nonetheless, many countries are still lacking electricity and the way energy is nowadays mainly produced cannot be claimed to be clean or sustainable.

While worldwide huge efforts are made to move from coal, oil, and gas as main energy sources towards renewable energies like wind, solar and geothermal, a major issue comes naturally out. If renewable energies hit the target for what concerns sustainability, they fail from the start if they are used to provide a baseload power (not-varying in time) to the grid. In fact, their output power can vary drastically at a moment's notice. That is probably one of the main reasons why energy is still mainly produced from fossil fuels (see **Figure 1**). Therefore, while renewable energies are warmly welcomed in the energy landscape and research will hopefully make them ever more reliable and competitive, we presently need some other clean sources of energy.

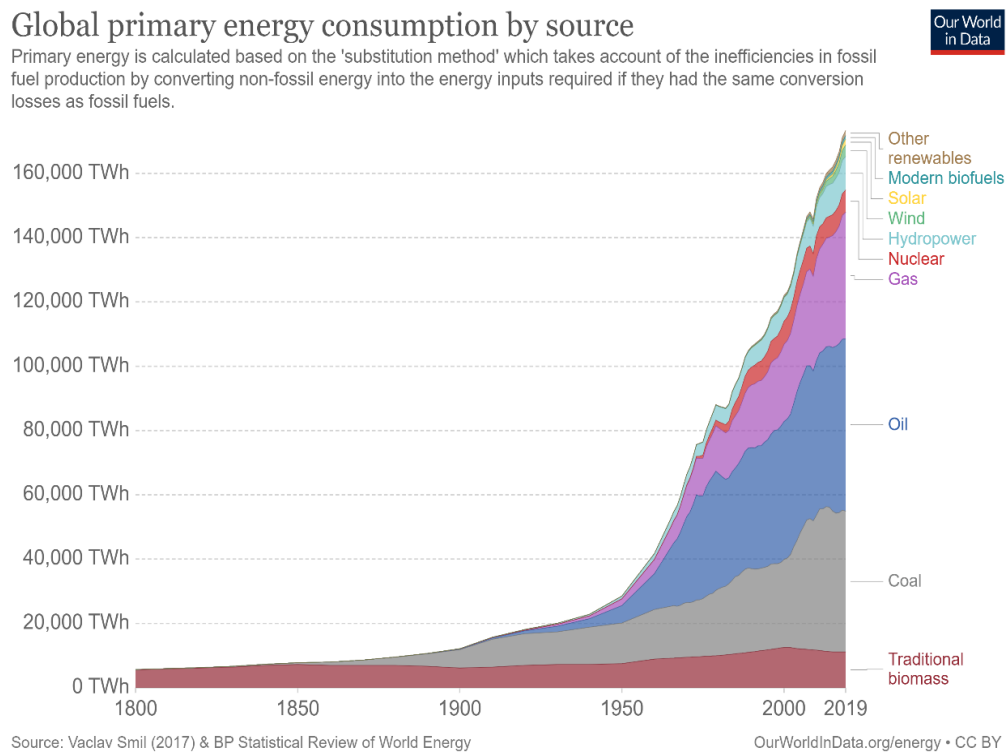


Figure 1 - Global primary energy consumption by source [1].

And here comes nuclear energy and its two energy applications. The first, fission energy, is presently worldwide exploited and while its physics and technology are well-established, many social acceptability aspects, mostly related to environmental and safety issues, have not been solved yet. The second, fusion energy, is currently the object of study of several research institutions around the world. Investments in this fields are coming from billionaires, like Jeff Bezos, venture capital firms, philanthropists and even oil and gas companies [2], even though its physics is not totally understood yet, and many technological and engineering challenges still lie ahead preventing it from becoming a competitive clean stable source of energy.

What is fusion? When two atoms bump against each other with an energy capable of overcoming the strong repulsive forces that naturally arise when they try to get closer, a fusion reaction takes place, and an enormous amount of energy is released. None of this was known until a hundred years ago, when, in 1920, Arthur Eddington advanced the theory that stars were actually fusion-driven bodies [3]. Thanks to his and to other scientists' later studies, it is now common knowledge that on the sun, atoms of hydrogen fuse continuously together thanks to the enormous gravitational field which pushes the particles one against the other. Unluckily, on earth, where the gravitational field is much lower, fusion reactions have a harder time. In fact, for a fusion reaction to take place, the temperature of the gas mixture must be around 150 million Celsius degrees, about ten times the temperature of the centre of the sun.

As mentioned above, whether on the sun, or on the earth, when somehow two atoms fuse together, an incredible amount of energy is released (17.6 MeV, see Eq. (1.1)).



In Eq. (1.1) is represented the fusion reaction that stands behind the DT curve of Error! Reference source not found..

In **Figure 2** are shown the fusion cross-sections for different types of reactions as a function of the required gas temperature (1eV ~ 11604,5 K). The DT (Deuterium-Tritium) reaction appears to be the most promising for at least two reasons. First, fixing a value on the y-axis, DT features the lowest activation temperature. Second, in the range of technologically achievable temperatures (setting to 5.5 trillion degrees K, ~500 keV, the upper limit [4]), DT reaction rate (the cross section) stands well above its rivals.

In the 1950s, when Mark Oliphant demonstrated the possibility of replicating a hydrogen fusion reaction in laboratory [3], researchers around the world started looking for the possibility of building a machine to control the frequency of this reaction and extract the energy released by it. Various projects have henceforth come to light.

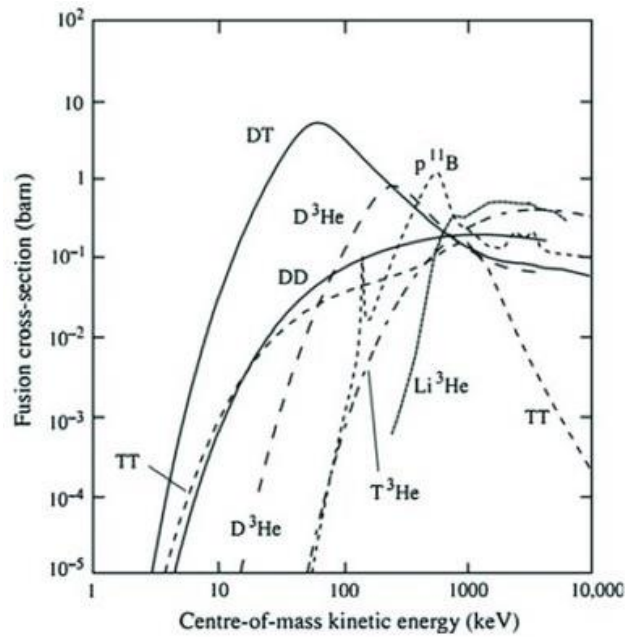


Figure 2 - Fusion cross-section for different types of reactions as a function of the kinetic energy of the gas [5].

Defining as fusion ignition the moment in which a controlled fusion reaction produces more energy than what it absorbs, different approaches are being currently studied to achieve it:

- Inertial confinement fusion. An example is the work carried on by the National Ignition Facility [6], in which very powerful lasers are used to heat up a mixture of DT.
- Magnetized target fusion. An example is the work by General Fusion [7] in which steam powered pistons are used to compress a magnetized DT mixture.
- Magnetic confinement fusion. An example of this technology application is the ITER (International Thermonuclear Experimental Reactor) project [8]. Plasma hydrogen (a fully ionized state of matter produced by heating up and compressing a DT gas) is magnetically confined by massive electro-magnets.

The third idea alone is of interest for the scope of the present work. Of all the proposed configurations, two are in vogue nowadays: the tokamak and the stellarator devices (see **Figure 3a** and **Figure 3b** respectively), the first more widely studied than the second.

Both tokamaks and stellarators are doughnut-shaped devices that solve the first main issue of fusion (confinement) using strong electro-magnets to confine, compress and shape the plasma. The second main issue (heat transfer) is mainly carried out by the blanket, where energy is extracted from incoming neutrons (that escape magnetic confinement being neutrally charged) and transferred to the coolant. Blanket is also there to protect the outer parts of the machine from plasma. When plasma is hot enough, and fusion reactions start taking place, neutrons will escape from the reactor, while the alpha-particles

(see Eq. (1.1)) will release their energy to the plasma, and that is why tokamaks and stellarators can in principle be self-sustaining devices. Now, the two devices are actually very different when talking about size, geometry, and operating conditions. Tokamaks have three main types of magnets (see **Figure 3a**). Toroidal field (TF) coils are meant to generate the toroidal magnetic field. The central solenoid (CS) is designed to work like the primary winding of a transformer and thus induce a current in the plasma (the secondary of the transformer), which generates the necessary poloidal magnetic field to guarantee the plasma stability. The poloidal field (PF) coils are there to give the desired shape to the plasma. And here is the first main difference between the two devices. Stellarators toroidal field coils are shaped in such a complex way that they take full care of the plasma confinement and shaping. Thus, they do not need a CS to induce a plasma current and can work in steady-state conditions. On the other hand, being the tokamaks based on the transformer principle, they ought to work in pulsed mode, which is not desirable to produce a base-load power.

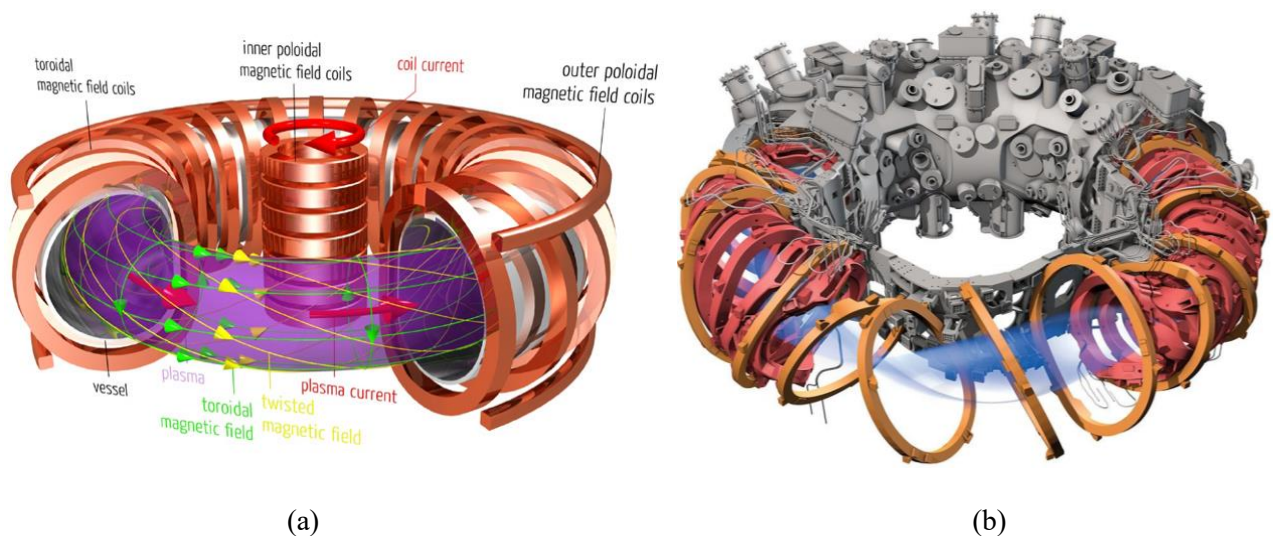


Figure 3 – Shape of the Tokamak (a) and Stellarator (b) plasma and magnets, [9], [10]. Although the two devices look similar in size, they are usually very different in reality.

Notwithstanding this nice feature of the stellarators, their geometry is awful and thus magnetic fusion scientists are concentrating almost entirely on the development of tokamaks. Size also is of interest for the comparison. If for example a comparison is made between the two present-day major exponents of the two types of devices, e.g., ITER vs Wendelstein 7-X, the first outweighs the second by 28:1 [11], thus making, in principle, stellarators less expensive than tokamaks. A more detailed comparison of the two devices can be found in the work by Yuhong Xu [12].

But what about the fuel? According to a study by Garry McCracken and Peter Stott [13] deuterium (D), the first ingredient of the fuel mixture, can be easily extracted from water by a procedure called

electrolysis and one gram will produce 300 GJ of electricity. They also estimate that in the oceans there are 10^{11} tons of deuterium available. Looking at Error! Reference source not found., in 2019, the energy demand has been of about 170000 TWh which is equivalent to about $6 \cdot 10^{11}$ GJ. Thus, to cover the world energy demand it would require ~ 2000 tons of deuterium. Which compared to the total availability is a negligible quantity. So far so good. The second ingredient for the fuel mixture is tritium (T). Also known as hydrogen-3, it is a rare radioactive isotope of hydrogen. Being its half-life of about 12.32 years [14], there are no natural reservoirs on earth. Even though some tritium can be found in natural water, the most efficient way to produce it is through the following nuclear reaction involving Lithium-6:



Tritium is being currently produced in CANDU-type fission reactors when neutrons interact with the D_2O moderator and coolant. Each nuclear reactor of that type generates on average 130 g of tritium a year [15]. Since future reactors start-up inventories are of the order of ~ 1 kg and the current global tritium inventory is just of about 40 kg [16] and it is decreasing, future nuclear fusion reactors like DEMO [17] are being designed to breed T, i.e., produce more tritium than what they require to be operated, and so both self-sustain themselves and produce tritium for the start-up of other reactors. This operation will be carried out by a special type of blanket, the breeding blanket.

Once the device-type has been figured out, fusion ignition is achieved, heat is captured by the breeding blanket and transferred to the coolant, how electricity is generated? Well, that is the easiest part. As soon as there is a fluid carrying thermal energy, whatever type of thermodynamic cycle can be coupled to the reactor, to transform that heat into electricity.

People are investing their money and energies in this field because if everything goes well, a new clean, safe, and sustainable source of energy will eventually enter in the energy landscape. Clean because the future power plants based on this technology do not emit any CO_2 nor greenhouse gases, safe because the radioactive level of the plant would be far lower compared to the ones recorded in fission power plants and because the magnetically confined machines show in principle a negligible risk, i.e., they automatically shut down as soon as something goes wrong; and sustainable because the required fuel ingredients are either infinite or bred by the plant itself.

1.2. Needs for refrigeration in nuclear fusion

The stronger the magnetic field produced by the electromagnets in a tokamak, the better the confinement, the smaller the plant, and so the cost. But electromagnets work on the physical principle that an electrical current passing through a wire, generates a magnetic field. Thus, in general, the stronger the current, the stronger the magnetic fields. Of course, for each type of material there is a maximum

magnetic field achievable, but this is out of the scope of the present work. What is instead relevant is the fact that high currents produce high heat depositions on the magnets due to Joule effect, according to the Ohm's law. And this heat must be removed not to compromise the magnet mechanical and physical properties. But how big this heat can get to be? Well, a rough estimate can be made with Ohm's law:

$$Q \propto R \cdot I^2 \quad (1.3)$$

where Q is the heat deposition on the magnets, R the electrical resistivity and I the electrical current. It is easy then to see that unless R is small or zero, the heat deposition on magnets carrying \sim MA of current is huge. According to Arnaud Devred, the former Superconductors and Cryostats Group Leader of ITER, if ITER used resistive (copper) magnets, something like 800 MW would be spent to operate them [18]. Which is clearly not a viable option. From 1911, when Heike Kamerlingh Onnes discovered superconductors (metals that below a certain temperature show zero electrical resistance and other properties [19]) until 1986 the resistive magnets have been substituted by the Low Temperature Superconductors (LTS). LTS are so called because they must be operated below \sim 20 K in order to exploit their superconducting properties. Examples of these superconductors are the NbTi alloy and the Nb₃Sn based strands (both are being used to produce ITER magnets, see blue parts in **Figure 4**).

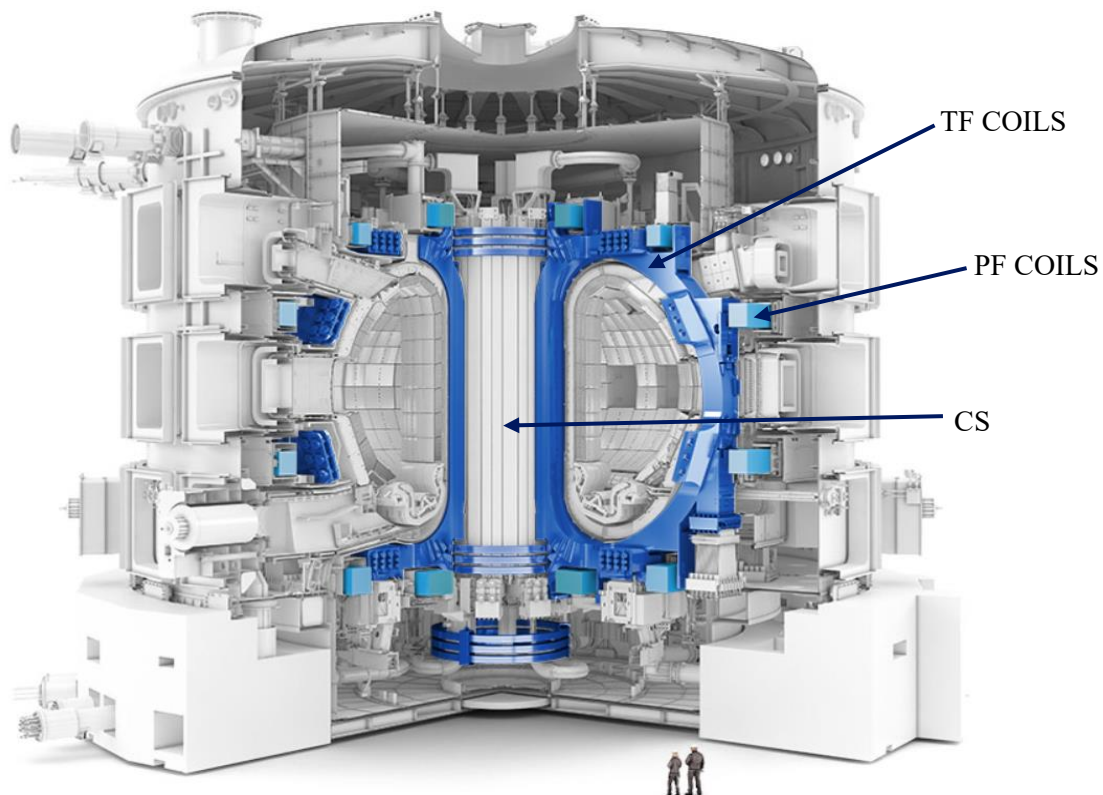


Figure 4 - Superconducting magnets system of ITER composed by Toroidal Field (TF) coils, Poloidal Field (PF) coils and Central Solenoid (CS) [20].

Although LTS allowed fusion research make a leap forward, another important breakthrough happened in 1986 when Müller and Bednorz discovered the High Temperature Superconductors (HTS) [21]. As the name suggests, they are superconductors with a high or very high critical temperature (temperature below which they ought to be operated to be superconductors). An example of HTS is the YBCO [22]. In **Figure 5** it is shown a comparison between the performance of three types of LTS (NbTi, NbSn, NbGe) and one type of HTS (YBCO). It can be appreciated the wider field of application of the HTS compared to the other category. While the maximum critical current density J of YBCO is comparable to those of the LTS, the HTS can be, in principle, operated at much higher temperature (~ 90 K) and can achieve incredibly higher magnetic fields B (~ 250 T). These last two features are desirable as they would decrease the reactor building costs (stronger B means smaller magnets required and therefore smaller reactors) and their operational costs (simpler and smaller refrigerator are required when the magnets operational temperature increases).

This type of materials brought new hope towards the possibility of producing energy from fusion. In fact, if the electrical resistance drops to zero, they will not experience any heat deposition.

Although research on HTS have made great progresses [23] and in the future they will probably replace LTS for fusion applications, presently most applications still use low temperature superconductors. As mentioned above, ITER magnets will all be composed of LTS. The adopted technique to build its magnets is called CICC (Cable-In-Conduit-Conductors).

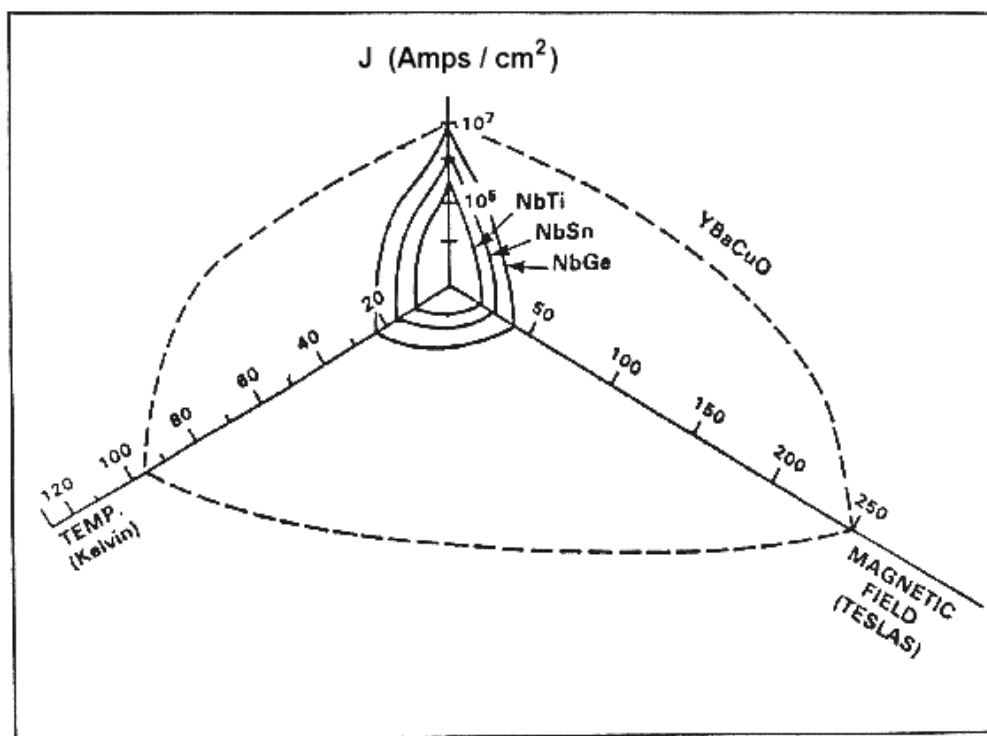


Figure 5 - LTS (NbTi, NbSn, NbGe) vs HTS (YBCO). Comparison of the phase diagram for two categories of superconductors [24].

In **Figure 6** it is schematically represented the complexity of the CICC technology. Each magnet is wound with one or more CICCs [25]. Supercritical helium is then forced through the central channel and the cable region of the conduit to keep the magnet at the desired temperature (~ 4.5 K).

Therefore, a suitable cryoplant has to be designed to guarantee that the magnets are kept sufficiently cold at all time. The cryoplant is composed by the He refrigerator, where the He is cooled from room temperature down to cryogenic temperature through the use of a properly designed thermodynamic (closed) cycle, the He loops, supplying the coolant to the different tokamak utilities at the required temperature level (e.g., supercritical He, SHe, at ~ 4.5 K sent to the magnets during cold operation), and the liquid He (LHe) buffer(s) used as interface(s) between the SHe loop(s) and the refrigerator in normal operation. The He refrigerator is a very expensive component: the plant cost is directly related to the nominal cooling power (and therefore to the plant size), while the electricity consumption is linked to the actual cooling power during operation.

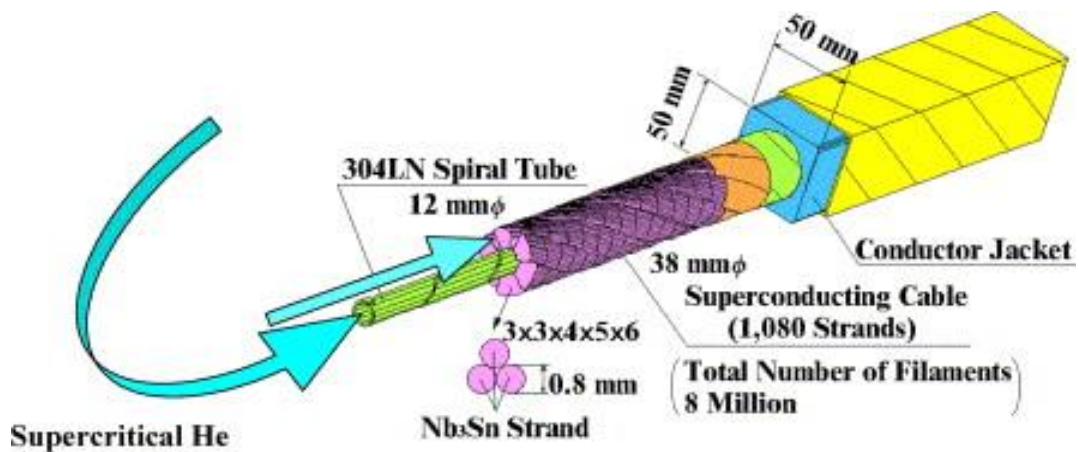


Figure 6 - Schematic representation of the CICC used for the ITER CSMC [25].

1.3.Existing fusion experiments and refrigerators

In **Table 1** a list of existing and forthcoming fusion experiments is collected, together with their refrigerator power and the main differences with respect to the ITER CSMC refrigerator, which is taken here as the reference model.

1.4.Existing refrigerator models and needs for modelling

Tools for the detailed thermal-hydraulic (TH) analysis of transients in superconducting (SC) magnets, such as the state-of-the-art 4C (Cryogenic Circuit Conductor and Coil) code [26], are available

nowadays. They have been validated (also predictively [27], [28]) in different transient conditions [29] including the cool-down (CD) [30], but they are usually not directly coupled to a suitable model of the refrigerator. Instead, they typically extend only to the heat exchanger between the LHe bath [31] and the primary SHe cooling-loop. The 4C code has already been employed for the analysis of the ITER Central Solenoid Model Coil (CSMC) CD optimization [32], although in the absence of a coupled refrigerator model the inlet He mass flow rate, pressure and temperature evolutions had to be imposed in input as boundary conditions (BCs). A first attempt to couple the CSMC to a simplified model of its refrigerator was attempted in [33] but the model was limited to the nitrogen pre-cooling stages. Also the pulsed operation of ITER [34] and JT-60SA [35] have been simulated by the 4C code, and various possible heat load levelling strategies have been explored [36],[37] using the code to model part of the HELIOS facility [38] at Commissariat à l'Énergie Atomique (CEA) in Saclay (France), but the upshot of the pulsed loads on the refrigerator has never been evaluated.

Moreover, existing refrigerator models are sometimes very complex and detailed [39], [40], and, as a result, computationally high-priced, or only partially validated [41], [42].

In view of the tight coupling between the refrigerator and the magnets, and of the necessity for optimization of this coupling, a dynamic He refrigerator model, fast running and able to quickly communicate (providing consistent BCs) with the state-of-the-art 4C TH magnet model, is thus essential.

Table 1 - List of some of the existing (and future) He refrigerators for magnetically confined fusion applications, including superconducting stellarators or tokamaks and experimental test facilities. The main differences with respect to the ITER CSMC refrigerator are also listed. HX stands for heat exchanger. See below for the description of the refrigerator components and topology.

Facility	Location	Refrigerator power at 4.5 K [kW]	Main differences vs. ITER CSMC refrigerator
JT-60SA TF coils cold test facility [43]	CEA, Saclay (France)	< 0.5 (~ 10 peak during CD)	- 4 HXs (one three-fluid HX) - the 2 isentropic expansions are not in series
ITER CC test facility [44]	ASIPP, Hefei (China)	0.5	- no three-fluid HXs - the 2 isentropic expansions are performed by piston expanders and are not in series
SST-1 [45]	Institute for Plasma Research, Gandhinagar (India)	~ 0.5	- JT valve replaced by a third turbine - single stage compression unit
Tore Supra [46]	CEA, Cadarache (France)	1 (0.3 at 1.8 K)	- three stages compression unit - production of superfluid He at 1.7 K
ITER CS final test station [47]	GA, San Diego (US)	~ 1	- single stage compression unit
EAST [48]	ASIPP, Hefei (China)	2	- JT valve replaced by a third turbine - 9 HXs (of which 5 three-fluid HXs and two four-fluid HXs)
ITER CSMC [49]	QST, Naka (Japan)	5	n.a.
W7-X [50]	IPP Greifswald (Germany)	~ 5	- 6 compressors (3-stages compression unit)
LHD [39]	NIFS, Toki (Japan)	~ 6	- 14 HXs (of which 8 three-fluid HXs and one four-fluid HXs) - 7 turbines - 8 compressors (2-stages compression unit) - no LN ₂ precooling
JT-60SA [51]	QST, Naka (Japan)	9	- JT valve replaced by a third turbine - 9 HXs (of which 6 three-fluid HXs and two four-fluid HXs) - 8 compressors (2-stages compression unit)
KSTAR [52]	NFRI, Daejeon (Korea)	9	- 11 HXs (of which 7 three-fluid HXs and one four-fluid HX) - 6 isentropic expansions - no LN ₂ precooling
ITER [53]	CEA, Cadarache (France)	75	- 10 HXs (of which 1 LN ₂ pre-cooler, 7 three-fluid HXs, two two-fluid HXs) - JT valve replaced by a third turbine

1.5. Aim of the thesis

The aim of this work is to develop the dynamic model of a He refrigerator and perform the preliminary tests of its capabilities to react to transients induced by heating coming from the client. To achieve this task, it is also necessary to build suitable Modelica dynamic models for the two-fluid and three-fluid heat exchangers that are used in most of the existing refrigerators (see **Table 1**).

1.6. The Modelica language

The Modelica programming language [54] is used here for the implementation of the object-oriented, dynamic model of the CSMC refrigerator. The same language has already adopted for the model of the magnets primary cooling loop, up to the LHe bath, in cryogenic circuit module of the 4C code [31]. Modelica obeys to a declarative paradigm and is highly modular, allowing an easy model development. The Modelica objects are organized in libraries. Starting from the components developed in the past for the analysis of the SHe loop of the SC magnet [31], the library has been extended to include the required components for the refrigerator model. The components contained in the resulting CryoModelica library either derive from the adaptation of components available in the open source Thermo-Power [55] or Modelica standard [56] libraries, see below, or are new, ad-hoc components, see **Figure 7**. The fluid properties (He and N₂, in the case of the refrigerator model) are taken from NIST [57] by means of the interface library External-Media [58].

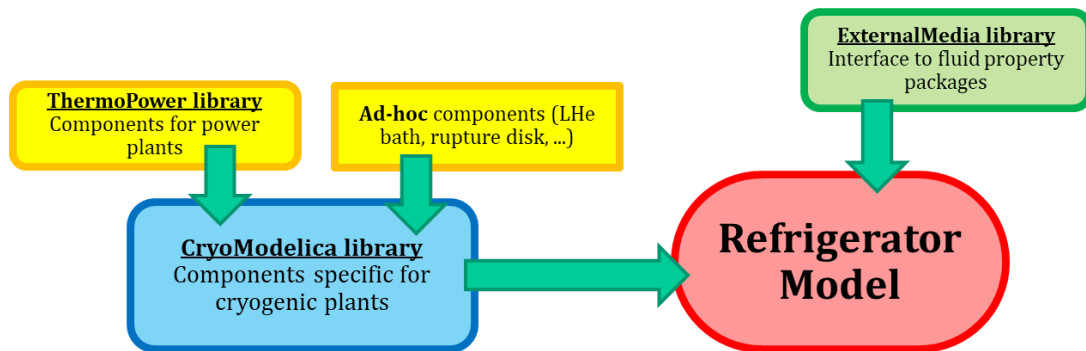


Figure 7 - Sketch of the relation among the different Modelica libraries (underlined), involved in the development of the refrigerator model presented in this work.

It is important to notice that with the Modelica language, every component has to be built in such a way that the number of unknowns is equal to the number of equations. Moreover, the interface variables, i.e., pressure, mass flowrate, enthalpy, between two connected components are set to be equal. In this way, when the total circuit is assembled, the number of equations will still be equal to the number of unknowns, so that the problem may have a solution.

2. Description of the Naka refrigerator

2.1. The naka CSMC facility

The CSMC refrigerator is designed to provide 5 kW of refrigeration power at 4.5 K for the cooling of the CSMC [59], of the insert coil (if present) and of their supporting structures. It was commissioned more than 20 years ago, so it is well known and established, and experimental data are available for a proper setup of the model inputs, as well as in the future to validate the model developed here.

2.2. Layout of the refrigerator

The CSMC He refrigerator features a conventional thermodynamic Collins cycle (the scheme in normal, cold operation is reported in **Figure 8**) with LN₂ precooling, two isentropic turbo-expansion stages connected in series (which distinguish the Collins from the single expansion typical of the Claude cycle [60]), and 3 Joule-Thomson (JT) isenthalpic expansions (see JT1, JT2 and JT3 in **Figure 8**).

The compressor unit is located on top of Error! Reference source not found. It is composed by a two-stage warm compressor, with inter- (and post-) cooler (IC and PC, respectively) HXs. The first low-pressure (LP) stage includes three screw compressors connected in parallel while the high-pressure (HP) stage features a single screw compressor.

Below the compression unit there is the Cold Box 30 (CB30). It contains the other, colder refrigerator components, i.e., the HX1-8, the turbo-expanders, and the JT valve, plus the temperature, pressure and flow sensors and the control equipment. The gaseous He (GHe) is pushed out of the compressor unit and driven through a series of 3 HXs (the pre-cooling stage, HX1-3 in **Figure 8**), the first two of which featuring LN₂ pre-cooling; in the CSMC refrigerator, the LN₂ is stored in a proper tank and vented to the atmosphere after it has been used. The He then enters the cooling stage, composed by a series of 3 HXs (HX4-6 in **Figure 8**) in parallel to the two expansion stages, i.e., the turbo-expanders TE1 and TE2. Eventually, the He is driven to the 2 after-cooling stages (HX7-8 in **Figure 8**), where the expansion in the JT valve takes place.

The He finally reaches the client to be cooled; in normal (cold) operation, the client of the refrigerator is the CB40 (see **Figure 8**), namely the cryogenic pump unit. It contains the LHe saturated bath (He Bath) (thermally coupled by two HXs to the SHe loop cooling the CB50, i.e. the cryostat containing the magnets), the second JT valve (producing the LHe for the saturated bath) and the cold circulator of the SHe loop.

Cold He is then sucked out of the HeBath by a cold compressor (CC) which sends it up towards the HX series and the compression unit.

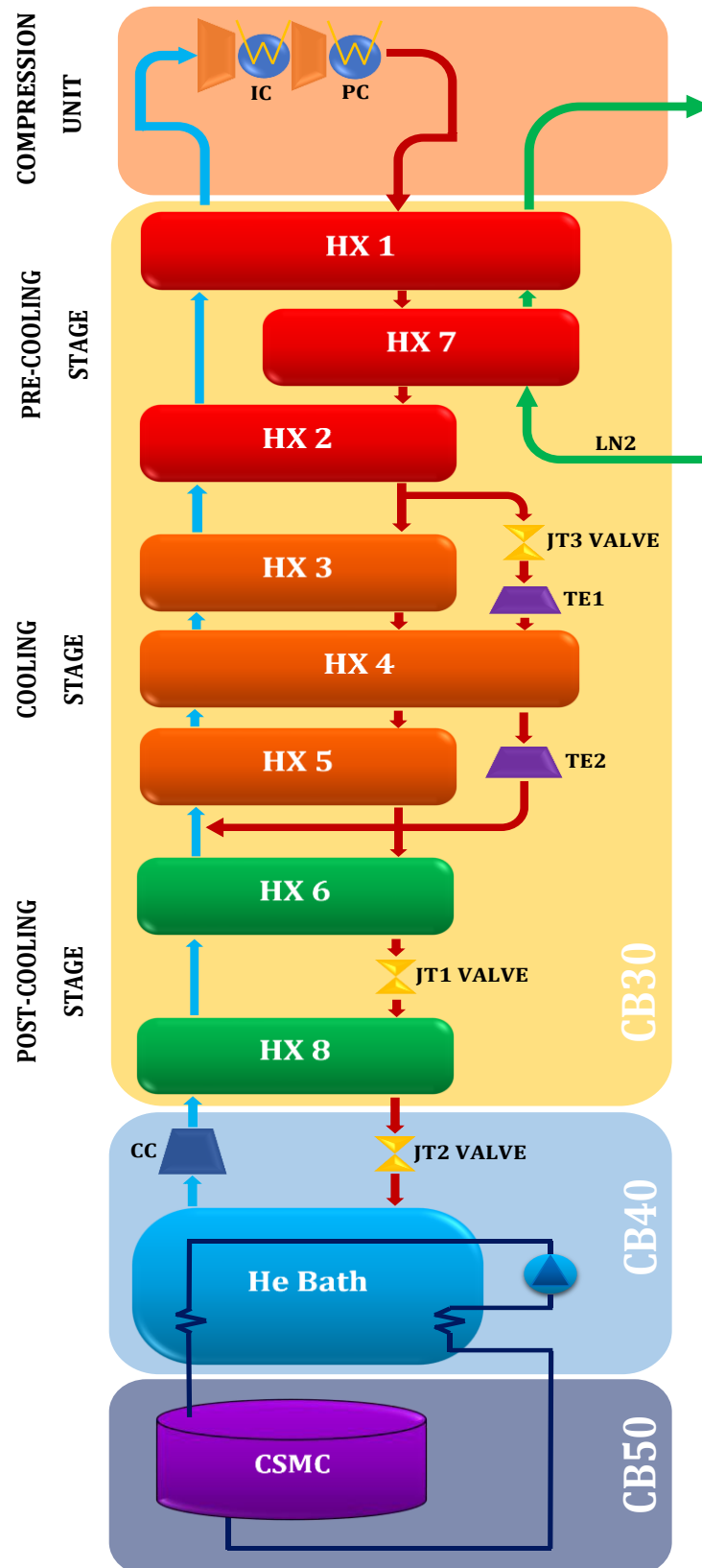


Figure 8 - Scheme of the Collins cycle adopted in the ITER CSMC He refrigerator during normal (cold) operation. Boxes from top to bottom: compressor unit, cold box (CB30), cryogenic pump unit (CB40), cryostat (CB50).

The thermodynamic cycle and most of the CSMC refrigerator features are fully representative of the refrigerators used in several existing and future tokamaks and test facilities, see **Table 1**, in terms of global configuration, i.e., pre-cooling, expansion and after-cooling sections. Indeed, the differences in the layout of the refrigerators reported in **Table 1** can be effectively modelled with the components developed here for the CSMC refrigerator.

2.3. Typical operational transients

From the magnets point of view, at least two normal operation transients involve a tight coupling with the refrigerator, namely:

- The cooldown (CD) from room to operation temperature, performed before starting the magnets operation. It is a slow transient, lasting up to several weeks depending on the mass of the magnet, actively driven by the refrigerator that supplies the He directly to the coil. Optimization of such a transient by means of simulations might be useful to reduce the CD time, while still satisfying the requirements for a safe cooling of the magnet (i.e., a maximum temperature difference of 40-50 K between any two points of the magnet at any time during the transient [61]).
- The transient driven by the coil cold operation, much faster than the CD (developing on the minutes-hours time-scale), with the associated pulsed (nuclear + AC, in the case of a tokamak) heat loads acting on the magnets. This transient is passively suffered by the refrigerator, which provides LHe to a bath used as heat sink/thermal buffer by the primary cooling loop of the magnets, usually cooled by SHe. In order to avoid expensive dimensioning of the refrigerator on the peak heat load, suitable smoothing strategies are required, which can be developed either in dedicated test facilities, see e.g. [37], [38], or by means of reliable numerical tools [62], [63], [36], [37].

Here the model is targeted at the simulation of the latter operation mode.

3. Refrigerator model

Most of the components needed to assemble the refrigerator, e.g., the HeBath or the JT valves, were already available in the CryoModelica libraries. Two things were missing though, and here is the crucial point: the first was a working dynamic model for the 2-fluids and the 3-fluids HXs, while the second was a “closed-loop” dynamic model of the entire refrigerator. First stage of the design process consisted in a very delicate and laborious analysis of the physics and geometry of the reference real HXs. When all the needed parameters were deducted, guessed, or calculated, the modelling phase initiated. Starting from pre-existing elementary components, whose models have also been thoroughly analysed, very complex models for the HXs have been designed, assembled, calibrated, tested and inserted in the circuit. This latter part proved to be quite demanding, as this type of plant (the He refrigerator) is very “sensitive” to small changes, i.e., every single parameter modification (and each component of the circuit has many input parameters) affects largely the behaviour of all the other components. Therefore, whenever a new component was added to the previous modelling stage, all the other components parameters had to be checked and often modified. To have a better understanding of what that means, in **Figure 9** are shown some screenshots taken during the modelling phase. The starting point was a “simple” model featuring the He Bath, JT2 and the CC (see top-left picture in **Figure 9**). After all the input parameters were given, the circuit was tested and the results were satisfying, another major component (see top-right picture in **Figure 9**) was added, along with some marginal components (temperature sensors, localized pressure drops, etc.), and so on and so forth. A mass-flow source and a pressure sink were added to the extremities of the circuit and moved progressively up, until the circuit was closed and completed.

The inlet (solid) and outlet (hollow) circular connectors (see for example **Figure 10**) are used to exchange the three interface variables (pressure p , mass flow rate dm/dt and specific enthalpy h) between the various components. Each connection, identified graphically by the straight blue lines in **Figure 10** and **Figure 11**, defines two equations:

- p , an “effort-type” variable, is prescribed to be the same in linked connectors.
- the sum of the dm/dt (a “flow-type” variable, positive when entering the component) must be equal to zero.

The third interface variable, i.e., h , is a “stream-type” variable, which is advected from the upstream to the downstream component.

The resulting circuit layout is reported in in **Figure 10** and **Figure 11**. The input data for the valves (JT1, JT2, JT3), Helium Bath (HeBath), warm compressors (C1 and CG1), cold compressor (CC), and turbo-expanders (TE1 and TE2) are reported in **Table 2**.

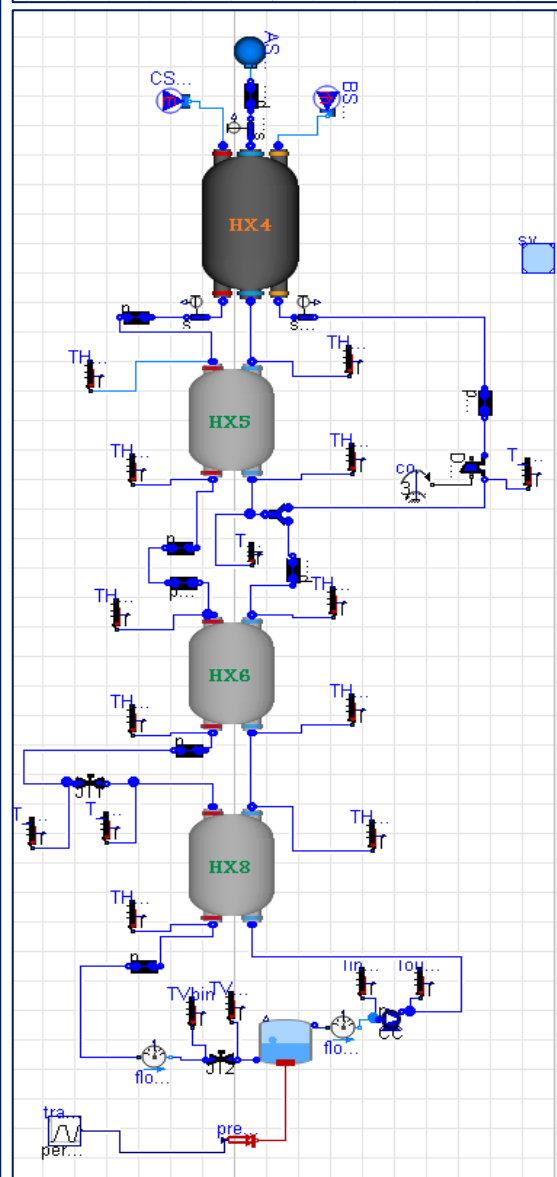
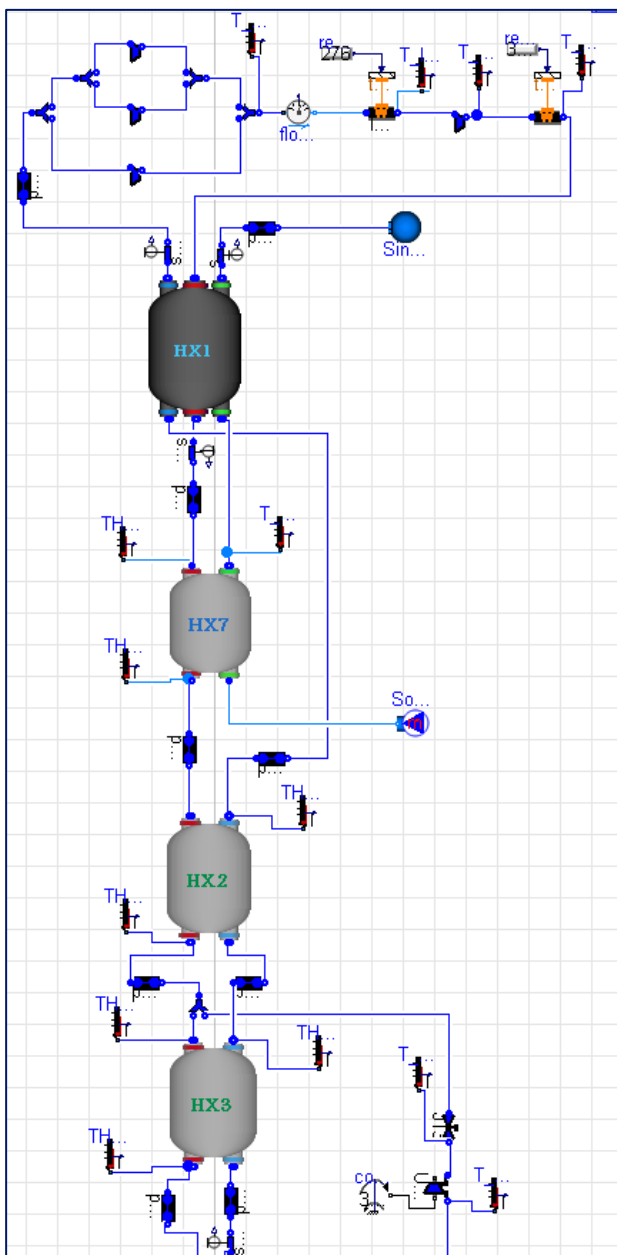
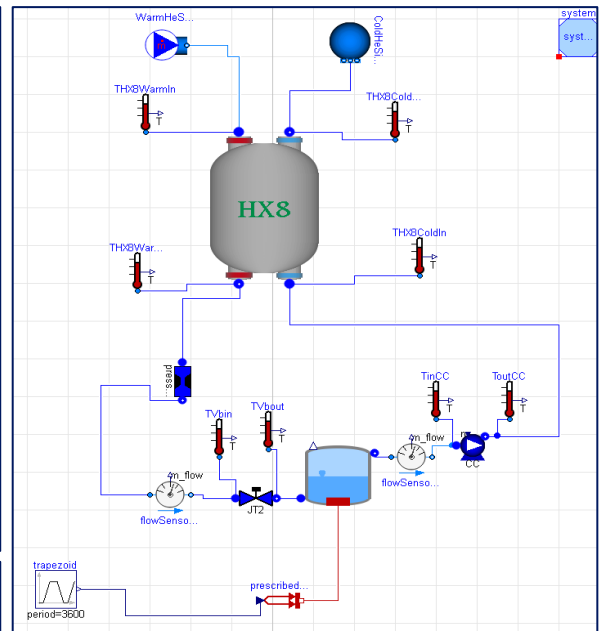
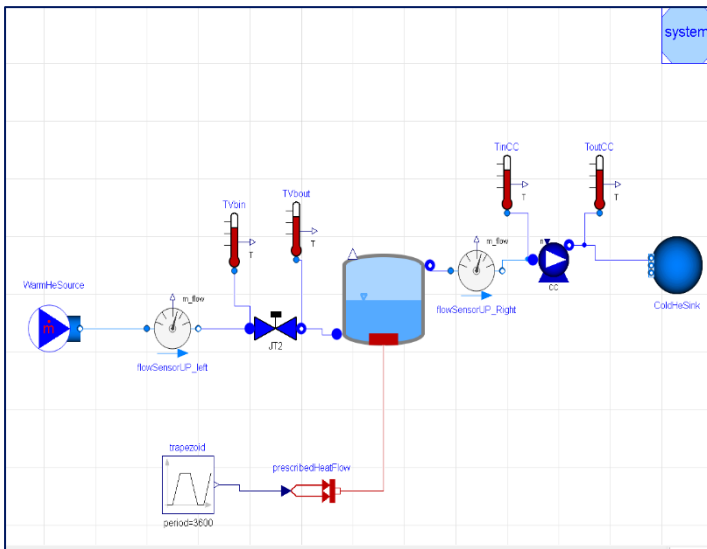


Figure 9 - Screenshots of various moments of the design stage. This picture are just meant to show the complexity of the system.

Most of them are taken from the data sheets provided by the manufacturer of the actual components (e.g., the operating point of the CC, or the dimensions of the HXs), from their nominal design values (e.g., the HeBath data) or from the settings adopted in the circuit (e.g., the opening of the valves). In some cases, the lack of such information is covered by well-educated guesses based on previous experience or experimental data. In particular:

- the value of C_v , rangeability and opening of some of the valves were guessed, starting from the operating conditions, as they are unknown and their influence on the computed results has been assessed to be negligible.
- the values of the geometrical parameters of the IC and PC HXs have been estimated in order to have almost ideal inter- and post- cooling stages, as it could be deduced from the experimental data.

the isentropic efficiency of the compressors ($\eta_{iso,C}$) and of the turbo-expanders ($\eta_{iso,T}$) has been obtained best fitting the experimental (constant) mass flow rate when constant boundary conditions (from nominal operation) are provided to the compressor system model.

Table 2 - Main input data of the He refrigerator model.

Component type	Component name	C_v		Rangeability (equal percentage) [-]	Nominal Opening [%]
Valve	JT1	12*		50	55*
	JT2	12*		50	70*
	JT3	12*		50	94*
		Length [m]	Number of parallel pipes	Diameter (inner/outer) [mm]	Cooling fluid temperature [K]
	HX IC	30*	180*	5.7* / 7.7*	276*
	HX PC	30*	180*	5.7* / 7.7*	309*
		TPR (p_{in}/p_{out})		$T_{in,nom}$ [K]	$p_{in,nom}$ [bar]
Turbo-expanders	TE1	2.4		36	16.00
	TE2	1.04		18.6	6.5
		$\eta_{iso,C}$ [%]		Control pressure [bar]	
Warm Compressor	CG1a/b/c**	65.1*		8.8	
	C2	96.9*		8.8	
		Nominal Inlet pressure $p_{in,0}$ [bar]		Nominal pressure increase Δp_0 [bar]	
Cold Compressor	CC	1.21		0.01140	
		Volume [m ³]		Initial Liquid Level [%]	Initial Pressure [bar]
Helium Bath	HeBath	23		70	1.21

* The value was guessed based on previous experience or deduced from experimental data, since it was not available.

** CG1a, CG1b, CG1c are the three parallel compressors composing CG1.

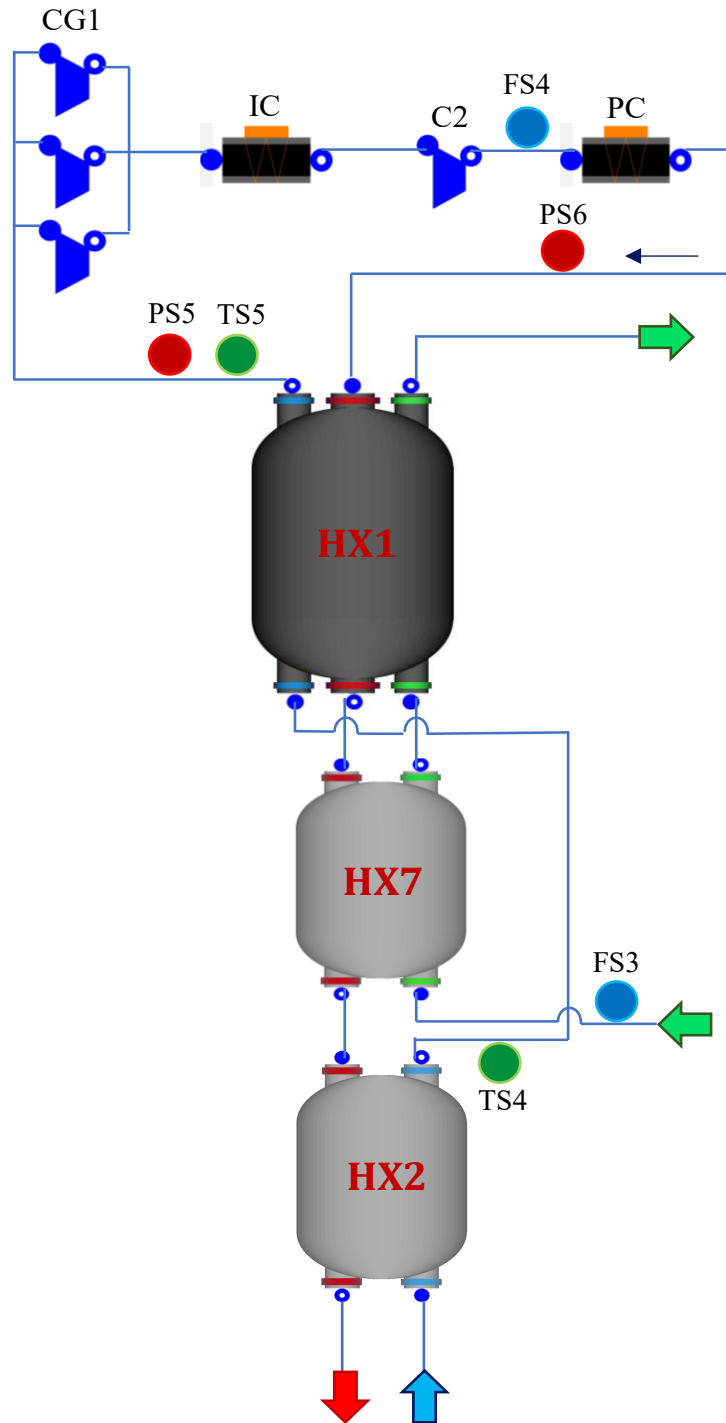


Figure 10 - Refrigerator model: N_2 pre-cooling stage. The red arrow stands for the warm He being cooled, the blue one for the cold He being heated and the green arrows for N_2 . CG1 = Compressor Group 1, C2 = Compressor 2, IC = Inter-Cooler, PC = Post-Cooler. Blue, green and red circles are flowrate, temperature and pressure sensors respectively.

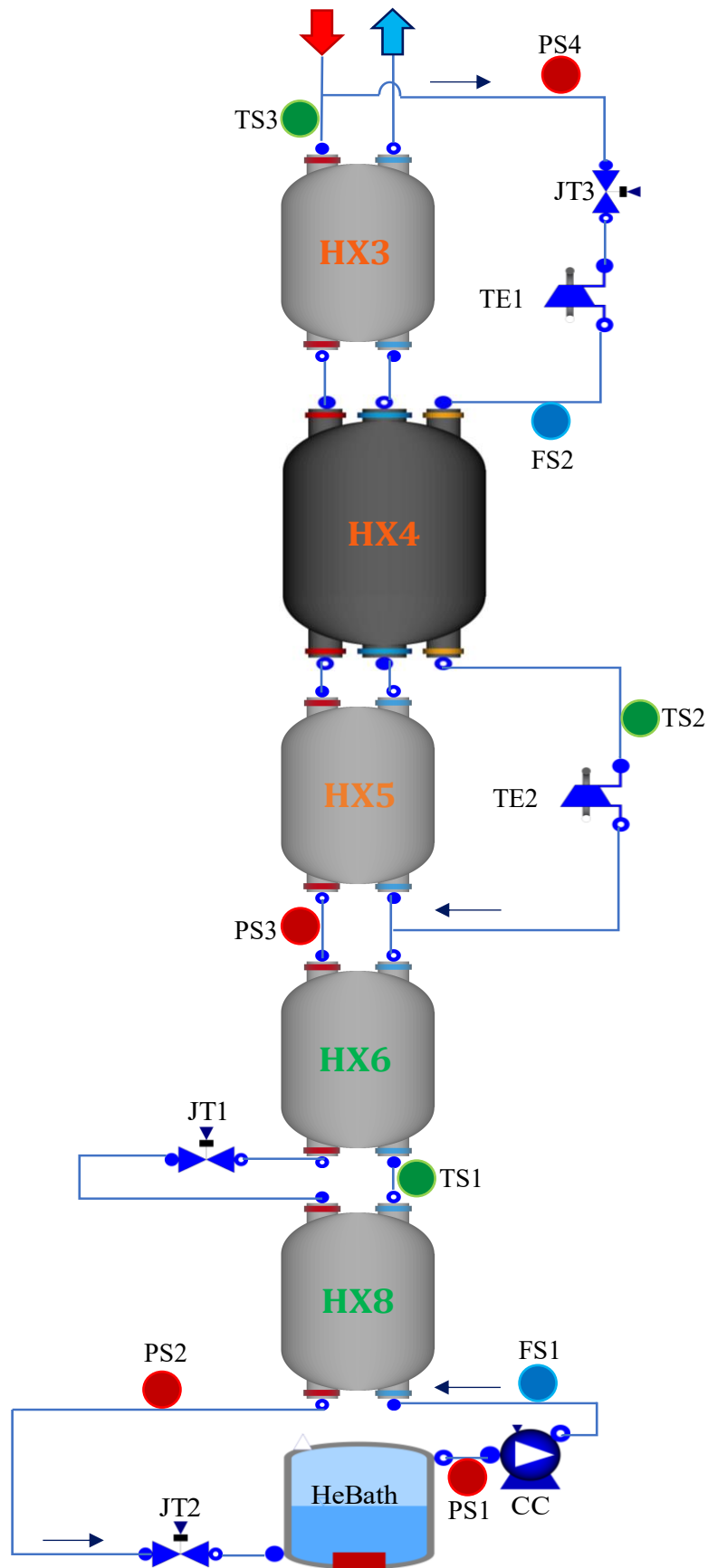


Figure 11 - Refrigerator model: cooling and post-cooling stages. TE1 and TE2 are the turbo-expanders, JT1, JT2 and JT3 the iso-enthalpic (Joule-Thomson) valves, CC the Cold Compressor and HeBath the Helium Bath. Blue, green and red circles are flowrate, temperature and pressure sensors respectively.

In **Table 3** are listed the nominal pressure, temperature and mass flowrate, read by some of the sensors along the refrigerator model (see **Figure 10** and **Figure 11**).

Table 3 - Refrigerator model sensors readings.

PS1 [bar]	PS2 [bar]	PS3 [bar]	PS4 [bar]	PS5 [bar]	PS6 [bar]
1.21	16.00	16.22	16.28	1.07	16.44
TS1 [K]	TS2 [K]	TS3 [K]	TS4 [K]	TS5 [K]	
11.9	18.6	36.0	83.5	308.0	
FS1 [g/s]	FS2 [g/s]	FS3 [g/s]	FS4 [g/s]		
416.98	178.00	37.065	594.98		

3.1. General modelling assumptions

The modelling assumptions that can be labelled as “general”, i.e., related to all the refrigerator model, are the following:

- Neither automatic nor manual controls of the valve openings are considered here. All the valves are operating with a fixed opening throughout the transient.
- CB50 and the related circuit of She, transferring heat to the HeBath, are substituted by an input heat flux, whose value can be changed by the user.
- The volume of the tubes connecting two components (HXs, valves, turbines, ...) is neglected (blue lines in **Figure 10** and **Figure 11**). This approximation is not far from the real case, where the components of the refrigerator are very close one to the other.

3.2. Description of the components

The description of the (existing and new) components used to assemble the refrigerator model is reported here. While the new components are described in detail, the characteristics of the pre-existing components are only summarized.

The definition of “input” and “output” for the components is only provided as an intuitive indication for the reader, as they are computed as solution of the differential-algebraic system of equations (of which both inputs and outputs are unknowns) at each time step, so that there is not a real (known) input and (unknown) output to each component.

This model does not claim to be the exact copy of the real refrigerator, as the controls and some minor and marginal components (for the simulation of the cold operation) have been excluded at this modelling stage, such as valves which are always closed or fully-open, He and N₂ tanks, gas purifiers, etc.

3.2.1. Cold compressor

In the refrigerator model the cold compressor (CC in **Figure 11**) is modelled using the “centrifugal pump” available in the CryoModelica library, which is an extension of the “PumpBase” in the ThermoPower library [55]. This latter model is based on the theory of kinematic similarity, i.e., the pump characteristics are given for nominal operating conditions (rotational speed and fluid density), and then depending on the similarity equations, they are adapted to the operation conditions.

Since no data for the CC was available, apart from the input and output expected values [64], its flow characteristic has been designed so that the CC may extract the desired quantity of He from the He Bath in nominal operating conditions. Starting from the nominal operating point (OP) (black asterisk in **Figure 12**), whose value has been figured out from the manufacturer’s data sheet [64], a quadratic characteristic has been constructed in order to avoid having the OP around the peak of the curve (so to avoid the possibility of having the CC operating in the surge zone, i.e., the region at the left of the peak).

A list of the input data of the CC is listed in **Table 4**.

Table 4 - CC input data.

Nominal inlet mass flowrate $\dot{m}_{in,0}$ (g/s)	Nominal inlet density $\rho_{in,0}$ (kg/m ³)	Nominal Inlet pressure $p_{in,0}$ (Pa)	Nominal pressure increase Δp_0 (Pa)	Nominal inlet enthalpy $h_{in,0}$ (J/kg)
416.89	20.24	121000	1140	20741.5

The CC model is based on the following equations:

1) energy balance equation:

$$\rho V \frac{dh}{dt} = \frac{\dot{m}_{in}}{N_p} h_{in} + \frac{\dot{m}_{out}}{N_p} h_{out} + W_{single} - Q_{loss} \quad (3.1)$$

where ρ is the inlet density of the fluid, V is the internal volume, h is the enthalpy, \dot{m} is the mass flowrate, N_p is the number of pumps in parallel, W_{single} is the power consumption of a single pump and, Q_{loss} is the heat loss of a single pump.

2) continuity equation

$$\dot{m}_{in} + \dot{m}_{out} = 0 \quad (3.2)$$

3) flow characteristic

$$y = -17.5e3 x^2 - 12.2e3 x + 88.9 \quad (3.3)$$

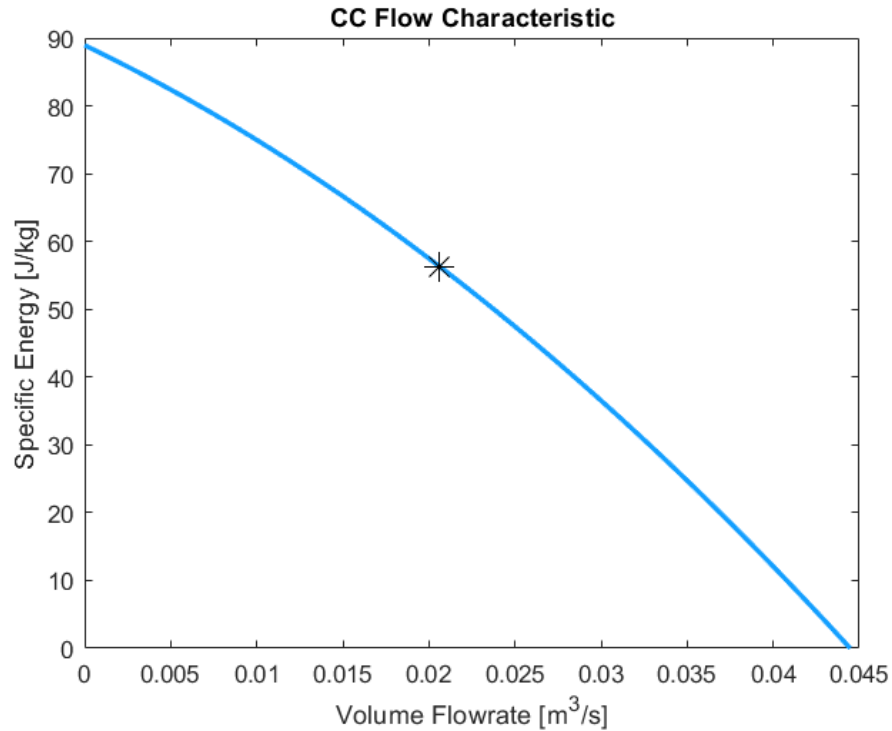


Figure 12 - Quadratic Flow Characteristic assumed for the CC.

3.2.2. Warm compressor

The warm compressor unit works at ambient temperature. In the reference CSMC facility it is a multi-stage compressor with inter and post cooling. The low density He enters the 1st stage, i.e., the low-pressure (LP) compressor, where it is equally split among the 3 parallel compressors (see **Figure 10**) operating between ~ 1 bar and ~ 9 bar. In the second stage, the higher density He is entirely driven through a single high-pressure (HP) compressor (C2). From the mechanical point of view, the component is an oil injected screw compressor [65], as adopted in most of the He refrigerators.

To model the compressors of the compression unit, the model “Compressor” from the CryoModelica library has been adopted. This model is based on the following assumptions:

- constant compression isentropic efficiency $\eta_{iso,C}$
- compression power linearly dependent from the control pressure $p_{control}$

- 0D component (the volume of He inside the compressor is neglected); as a consequence, the mass flow rate is the same at the inlet and at the outlet to satisfy the mass balance

The compressor operating conditions are defined by two inputs only: the linear compression power characteristic provided by the manufacturer, reported in **Figure 13**, and the isentropic efficiency value. In **Figure 13**, the control pressure p_{control} corresponds to the intermediate pressure of the two-stage compressor unit (namely, p_{out} for the LP compressor and p_{in} for the HP compressor).

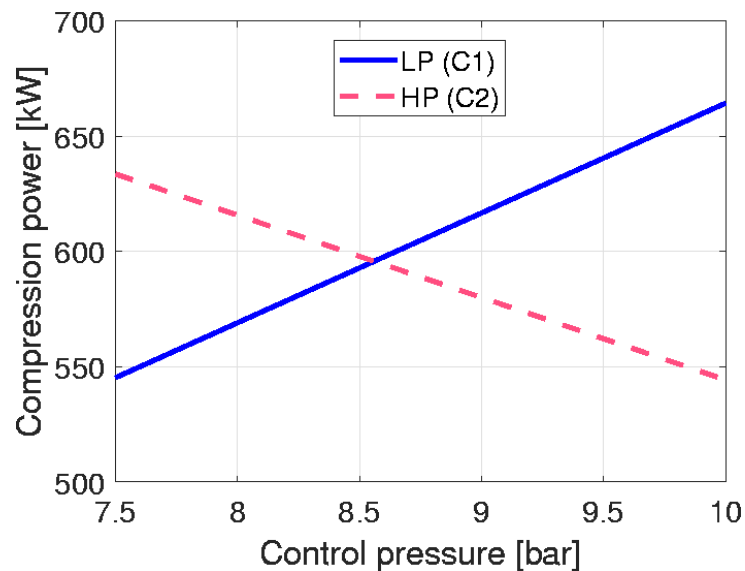


Figure 13. Characteristic curve (from manufacturer) of the CSMC refrigerator compressors.

The inter-refrigeration between the two stages (as well as the post-refrigeration) is modelled with the standard 1D HXs already available in CryoModelica.

3.2.3. Turbo-expanders

The refrigerator present at the Naka CSMC facility features two centrifugal turbo-expanders. Since the data provided by the manufacturer [66] have been slightly modified in order to obtain the desired pressure drops and temperature variations of the fluid passing through them.

The design of the two turbines has been carried out using the component “SteamTurbineStodola” from the ThermoPower library. Among the input requirements of the model there are (which were all guessed):

- Guy-Stodola coefficient
- Nominal pressure ratio
- Nominal isentropic efficiency

- Mechanical efficiency

3.2.4. Joule-Thomson valves

In the Naka refrigerator there are countless valves and as many varieties. In the present work only the main three valves are modelled (see JT1, JT2 and JT3 in **Figure 11**). They are designed based on the CompressibleValve model available in CryoModelica, based on the Industrial-Process Control Valves in ANSI/ISA S75.01. It accounts for the Joule-Thomson effect, i.e., a gas flowing through it is rapidly expanded and cooled down.

The Valve model requires in input, among other parameters, the following data:

- Cv flow coefficient
- Flow Characteristic
- Rangeability
- Opening
- Nominal inlet pressure

In view of the lack of manufacturer's information, Cv values and opening have been set in order to obtain the desired behaviour, e.g., JT2 has been set in order to keep the liquid level of the bath, see next sub-section, at the desired value.

3.2.5. SHe Helium Bath

This component plays a central role in the smoothing strategies adopted to cope with the pulsed load transients experienced by a refrigerator coupled with a tokamak. The supercritical helium buffer (or bath) has the objective of absorbing the thermal peak loads and progressively release the accumulated energy to the refrigerator.

In the refrigerator model presented here, this task is carried out by the "HeBath" component in CryoModelica. It is a 0D component that considers the phase separation of the contained fluid, i.e., liquid and vapour (which are also assumed to be in equilibrium with one another). It calculates the filling percentage of the liquid (and so of the vapour), and its value cannot be neither 0 nor 100% (completely filled with liquid or vapour), otherwise an error message is displayed when running the model.

An additional approximation has been introduced here, and it has to be taken into account when looking at the simulation results: the Naka CSMC refrigerator features three SHe baths, accomplishing

different although related tasks. In the present project, a single HeBath is utilized, with a total volume equal to the sum of the three baths volumes, i.e., 23 m³.

3.2.6. Heat exchangers

In the He refrigerator of the CSMC, the pre-cooling, cooling and after-cooling sections consist of aluminium plate-fin HXs, commonly used in cryogenic applications. They are compact-type devices composed by a stack of plates (partition plates or sheets) and a series of finned surfaces inserted between them to create small rectangular channels as shown in **Figure 14a**. He in different thermodynamic conditions (or He and N₂) flows in the channels of neighbouring plates (see **Figure 14b** for the 2-fluids HX and **Figure 14c** for the 3-fluids HX), so that the main heat transfer path is across the plates.

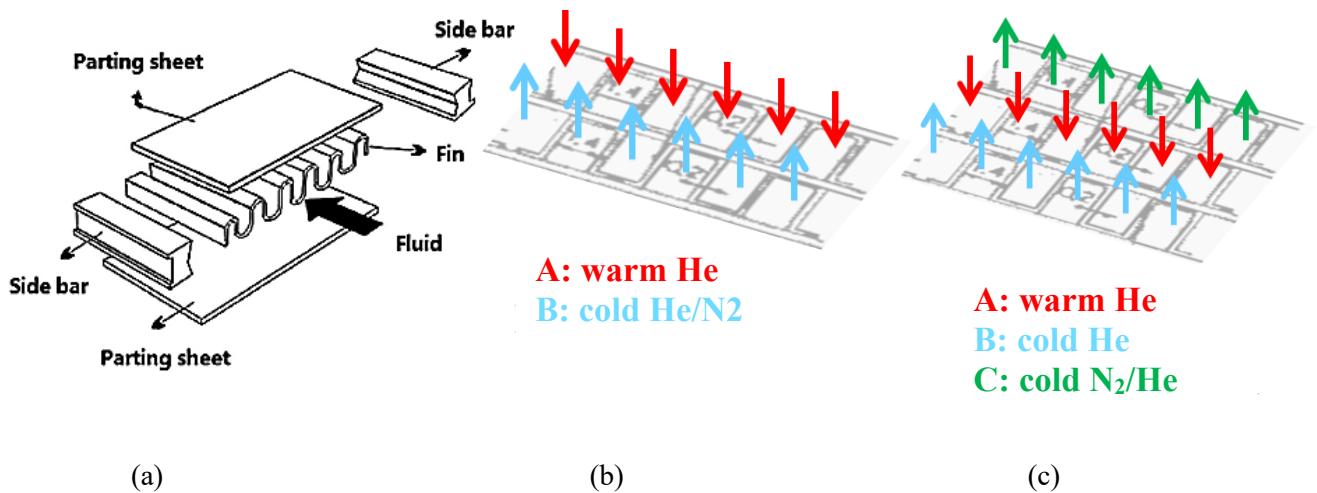


Figure 14 - (a) Plate-fin chamber (reproduced from Error! Reference source not found.), (b) and (c) sketches of the fluid flows in a two-fluid HX and in a three-fluid HX respectively, of the reference refrigerator.

The main assumptions on which the model is based include:

- a) Uniform aluminium properties (namely, the thermal conductivity).
- b) In the MetalWall component (see **Figure 15c**), available in ThermoPower which simulates the thermal behavior of a metal slab, the plate wall is considered as an ideal heat transfer wall (temperature does not vary within it).
- c) Absence of heat transfer among passages (rectangular channels among the fins) of the same fluid (within the same plate), e.g., any two adjacent channels with a blue arrow crossing it in **Figure 14b** and **Figure 14c**. For the 3-fluid HXs, it is also assumed no heat-exchange between the 2 heating fluids (in HX4) and between the two cooling fluids (HX1). This

assumption is based on the fact that two heating fluids (for HX4) or two cooling fluids (for HX1) are never in direct contact in the real HX.

- d) Suitable geometrical simplifications. The geometry of the HXs has been modified so that it was possible to join pre-existing and already validated models of single-fluid HXs from CryoModelica and produce “ad-hoc” multi-fluid HXs. Thus, what in reality are N rectangular conducts, in the model are treated as M circular pipes, where N is the number of channels provided by the manufacturer [64] and M has to be suitably chosen preserving the flow-areas of the fluids, the heat-exchange areas and the wetted perimeters (see below for more details).
- e) Constant global heat transfer coefficient (UA). It is an input value of the model. Starting from the reference value [64] the HX model is calibrated during the test-phase to get the expected output temperatures according to:

$$UA = \beta \cdot UA_{ref} \quad (3.4)$$

where β is the free parameter. The β values thus obtained are all around 2~2.4 for the 2-fluid HXs (He-He) and around 1.5 for the 3-fluid HXs (He-He-He). For the HXs featuring N₂, the values are smaller (HX7) or much smaller (HX1) (see **Table 6** and **Table 8**), and this is explained by the fact the N₂ has different thermal properties with respect to He, and its mass flowrate is much smaller than the He ones (see **Table 3**). Instead, the general increment of UA with respect to the real case can be explained by the fact that part of the heat transfer surface in the real case has been neglected here (see point c). For the 3-fluid HXs two values of β need to be evaluated, one for each thermal coupling between the fluids.

- f) No pressure losses throughout the HX channels. To compensate for that, localized pressure drops are spread along the circuit by suitable components from ThermoPower.

3.2.6.1. Two-fluid HX

3.2.6.1.1. Model

The model of the 2-fluid HX is schematically represented in **Figure 15**. The model layout is appreciable in **Figure 15c**. A “HeatedPipe” model (see HXWarm in **Figure 15c**) from CryoModelica is used to simulate the warm He to be cooled (it is a component only recently developed; a first numerical analysis, not reported here, e.g., on the number of nodes, has been made, showing promising results). Although it is represented as a single tube, it is actually a bundle of parallel pipes, whose number can be chosen by the user. All the geometrical parameters of the pipes can be set, as the diameter of the tubes, the thickness and also the walls material and the related thermo-physical properties. This bundle of pipes is thermally connected to the second bundle of pipes (HXCold), where the cooling fluid flows (He or N₂, in HX7), by a MetalWall. The latter component, as mentioned above, simulates the

thermodynamic behavior of a metal wall set as interface between two fluids. The MetalWall represents all the aluminum plates of the real HX. The element called “CoCu” in **Figure 15c** is there only to take into account the fact that the two fluids are flowing in counter current.

As shown in **Figure 10** and **Figure 11**, the He refrigerator is equipped with 6 two-fluid HXs:

- HX8, 6, 5, 3, 2 in which the HP He is cooled by the LP He
- HX7, where the HP He already pre-cooled in HX1 is furtherly cooled by heat transfer to the LN₂ from its storage tank.

In **Figure 16** the geometry and flow directions of the fluids in the HX are schematically represented. Each row of fins featuring the same fluid is called a *passage*. Defining the cold fluid as C and the warm fluid as A, looking at Error! Reference source not found.c it is shown how the passages repeat along the x-axis of the HX. Neglecting the two lateral passages Z, a total number of 78 passages is counted, 26 for C and 52 for A. Neglecting the heat exchange between two passages of the same fluid, there come out 52 plates taking effectively part in the heat transfer process.

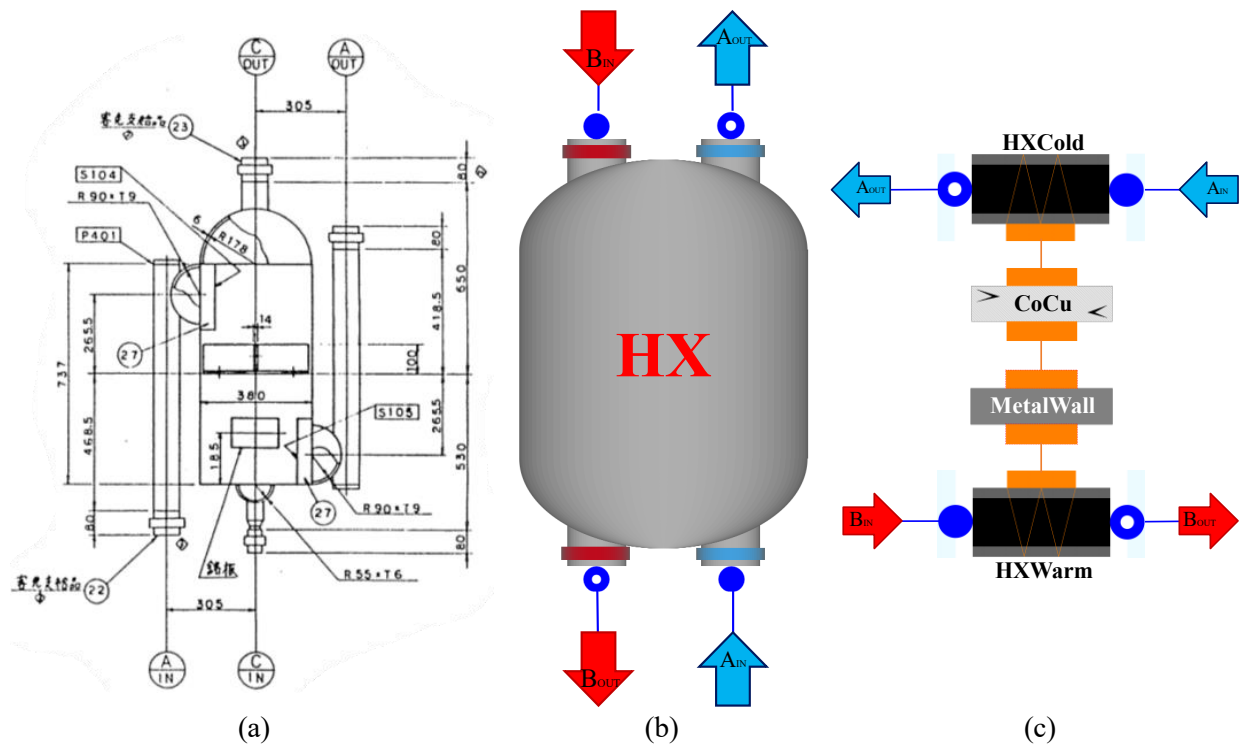


Figure 15 - (a) 2-fluid reference HX [64] (b) CryoModelica model HX (c) CryoModelica HX exploded view.

The warm fluid (He) to be cooled flows from top to bottom (red arrows) while the cold fluid (He or N₂) being heated flows in the opposite direction. Once the height, width, and depth of the HX interested in the heat exchange are figured out, and knowing the number of passages of the warm (52) and cold fluid (26), it is possible to calculate the following geometrical parameters:

The total volume (Al + fluids):

$$V_{tot} = w \cdot v \cdot L \quad (3.5)$$

The area of the total horizontal surface (light green part in Error! Reference source not found.a) (Al + fluids):

$$A_{tot} = w \cdot v \quad (3.6)$$

The area of the horizontal cross section of a plate:

$$A_{plate} = \delta_p \cdot v \quad (3.7)$$

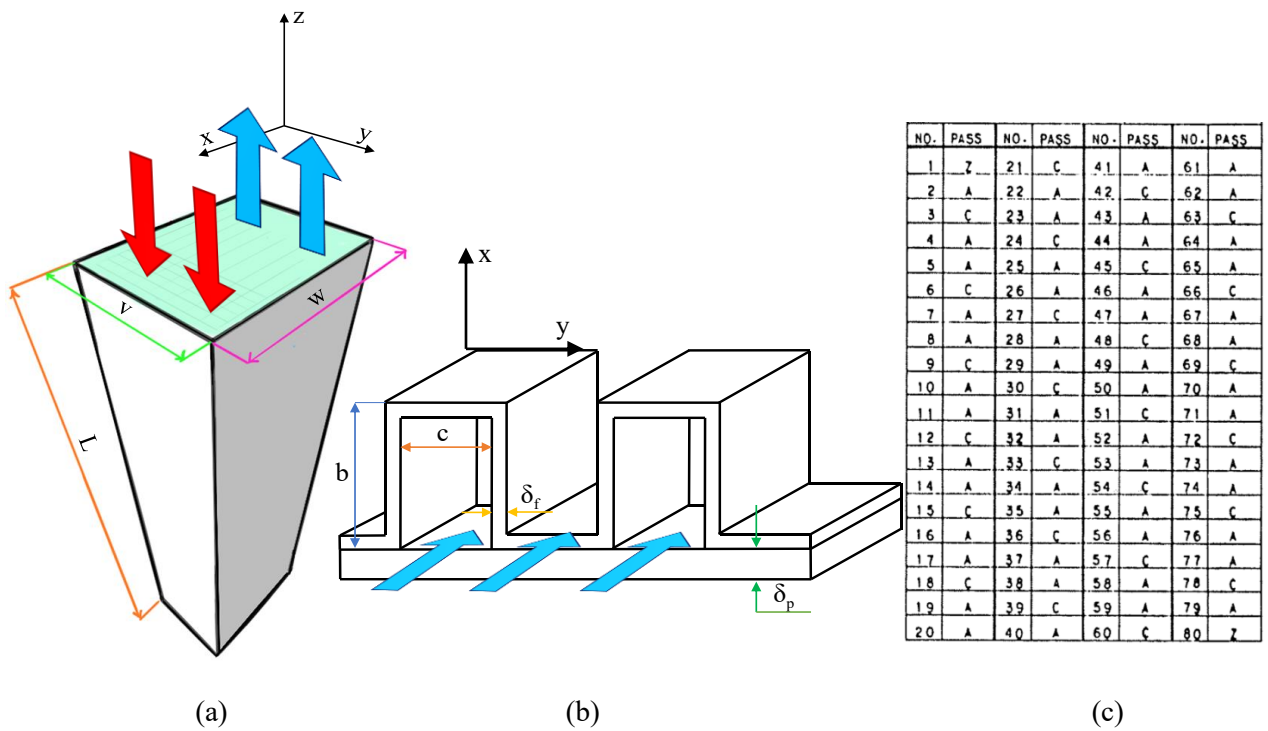


Figure 16 - (a) 3D sketch of the reference 2-fluid HX. (b) 3D detail of the recurrent pattern of the HX. This portion is repeated horizontally (along y) and is crossed by the same fluid. Then a horizontal plate separates it from another equivalent row of the same or the other fluid, on top / at the bottom of this row (along x plates and fins are alternated). The recurrence pattern is described in (c): a total of 80 passages is split between fluid A and C [64]. In this model only 78 passages are modelled, disregarding the 2 peripheral (Z) ones.

The area of the longitudinal (vertical) cross section of a plate (white part in Error! Reference source not found.a):

$$S_{plate} = v \cdot L \quad (3.8)$$

The area of the total horizontal surface of the plates interested in the heat transfer process:

$$A_{52} = A_{plate} \cdot 52 \quad (3.9)$$

And the area of the total horizontal surface of the plates left-out of the process:

$$A_{26} = A_{plate} \cdot 26 \quad (3.10)$$

Now, to compute the free-flow areas of the two fluids, the following process is adopted.

In **Figure 17** the repeated pattern of the fins is highlighted in green.

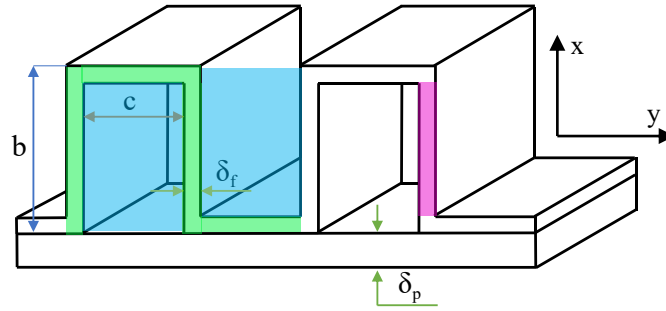


Figure 17 – Detail of the recurrence pattern in a passage.

In the width v there is room for 107.5 green patterns. In each of the 107 recurrent structures the available flow area is (blue part in **Figure 17**):

$$A_{flow,blue} = 2 \cdot (b - \delta_f) \cdot c \quad (3.11)$$

And the free flow area of an entire line is thus:

$$A_{line} = A_{flow,blue} \cdot 107.5 \quad (3.12)$$

The free-flow areas of the two fluids are easily calculated as:

$$A_{ff,A} = A_{line} \cdot 52 \quad (3.13)$$

$$A_{ff,C} = A_{line} \cdot 26 \quad (3.14)$$

As mentioned previously, the geometry of the HX has been modified in the following way in order to be used as input to the new, 2-fluid HX model of CryoModelica: the rectangular passages have been re-arranged in a certain number of circular tubes $n_{t,A}$ for the warm and $n_{t,C}$ for the cold fluid. The tubes have been designed so that the total free flow areas of the two fluids, and the total surface of heat exchange, are preserved. The following system was thus produced and easily solved:

$$\begin{cases} A_{ff,A} = n_{t,A} \cdot \pi \cdot R_{A,int}^2 \\ A_{ff,C} = n_{t,C} \cdot \pi \cdot R_{C,int}^2 \\ 2\pi R_{A,int} \cdot L = S_{tot} \\ 2\pi R_{C,int} \cdot L = S_{tot} \end{cases} \quad (3.15)$$

where S_{tot} is the total surface area taking part on the heat-exchange: $52 \times S_{plate}$ (white part in **Figure 16a**).

For this calculation the external radius of the tubes has been assumed same as the internal radius. The next step is to calculate the volume of the aluminium involved in the heat-exchange process:

$$V_{Al} = A_{plate} \cdot L \cdot 52 \quad (3.16)$$

This volume is used to evaluate the mass of the MetalWall (see **Figure 15c**) that is placed between the pipes.

The final step is to calculate the thickness of the pipes. Since not all the aluminium in the HX takes part to the heat-exchange process, the metal left out of the process will be distributed among the pipes as pipe wall.

The left-over aluminium is evaluated taking into account that in one line there are 215 pink parts (see **Figure 17**). Then the total area of these 215 parts is:

$$A_{pink,line} = 215 \cdot (b - \delta_f) \cdot \delta_f \quad (3.17)$$

And the total area is:

$$A_{pink,tot} = A_{pink,line} \cdot 78 \quad (3.18)$$

Now, this area of aluminium is summed to A_{26} and the total is proportionally split among the two set of pipes, so that the total Al volume (and thus its thermal capacity) is preserved in the dynamic model:

$$A_{Al,A} = \frac{2}{3} A_{pink,tot} \quad (3.19)$$

$$A_{Al,C} = \frac{1}{3} A_{pink,tot} \quad (3.20)$$

Then the external radii of the pipes are evaluated as follows:

$$R_{ext,A} = \sqrt{\frac{A_{Al,A}}{\pi \cdot n_{t,A}} + R_{int,A}^2} \quad (3.21)$$

$$R_{ext,C} = \sqrt{\frac{A_{Al,C}}{\pi \cdot n_{t,C}} + R_{int,C}^2} \quad (3.22)$$

In **Table 5** are summarized the main geometrical data of the real 2-fluid HX and of its model.

Table 5 - 2-fluid HX – Data

		Fluid A (warm)	Fluid C (cold)
Real 2-fluid HX	passages	52	26
	b (mm)	4.70	
	c (mm)	1.40	
	δ_f (mm)	0.20	
	δ_p (mm)	1.20	
	w (mm)	446	
	v (mm)	344	
	L (mm)	737	
	V_{tot} (m ³)	0.11	
	A_{tot} (m ²)	0.15	
	A_{plate} (mm ²)	0.41	
	A_{ff} (m ²)	0.07	0.03
Model 2-fluid HX	R_{int} (mm)	7.88	3.93
	R_{ext} (mm)	8.78	4.39
	n_t	362	723

3.2.6.1.2. Tests

The new 2-fluid HX model has been tested in nominal (cold) operating conditions and during this phase the parameter β has been calibrated in order to have the outlet temperatures as close as possible to the experimental results provided by the Naka CSMC facility [64].

In **Figure 18** it is shown the layout of the circuit in which the HXs have been tested. It is the same for all the 6 HXs. A mass flow rate source and a pressure sink for the cold fluid and the warm fluid are connected to the HX. The input mass flow rates are taken from the experiments [64]. In this way the circuit is closed, and the system of equations can be solved. The results are summarized in **Table 6**. To be noted that the experimental temperatures are not always reliable, so they are used as a general

reference for the calibration of the β parameter (e.g., HX7 in **Table 6**: the outlet temperature of the cold fluid appears to be higher than the inlet one, which is not physically possible).

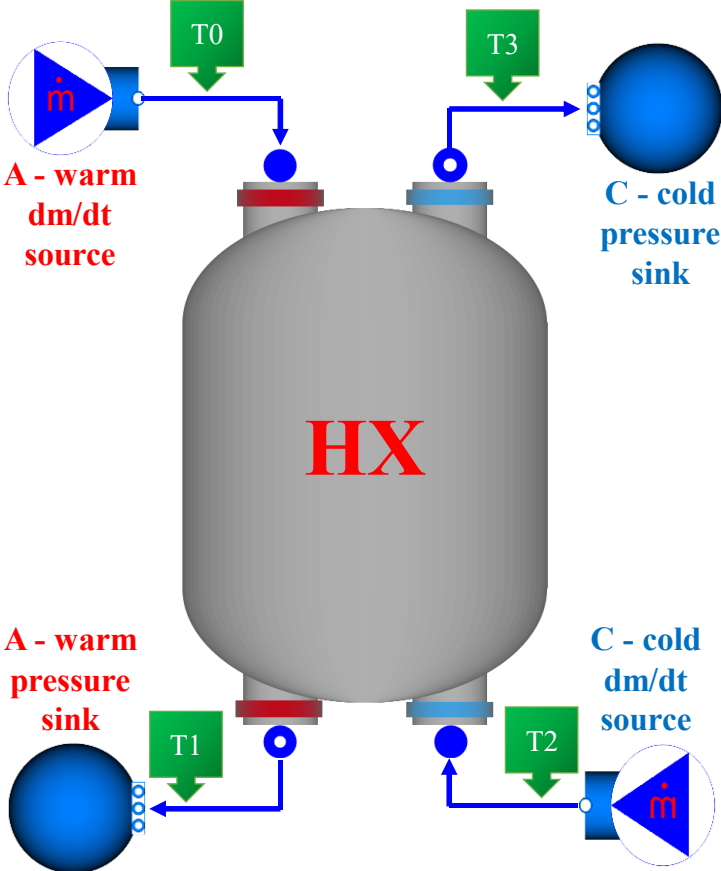


Figure 18 - 2-fluid HX model test layout. The path of the cold cooling fluid (He or N2 in HX7) is shown in blue. The path of the warm fluid (He) is shown in red. The temperature sensors are represented in green.

Table 6 – Comparison of the 2-fluid HX model test results with experimental data during the calibration of the β parameter. A summary of the 2-fluid HX test results are reported here. The relative difference with respect to the experimental measurements (in blue and red), minimized in view of the calibration, is also reported.

Result comparison 2-FLUID HX									
	β	T_{T2} [K]	T_{T3} [K]	$T_{T3,exp}$ [K]	err [%]	T_{T0} [K]	T_{T1} [K]	$T_{T1,exp}$ [K]	err [%]
H X 8	2.04	4.433	5.12	5.06	1.186	5.89	5.36	5.366	0.112
H X 6	2.35	5.06	12.01	11.9	0.924	12.24	5.75	5.8	0.862
H X 5	2.33	11.9	17.33	17.23	0.580	18.6	12.242	12.24	0.016
H X 3	2.27	28.08	33.75	33.57	0.536	36	28.48	28.59	0.385
H X 2	2.15	33.57	83.39	83.52	0.156	85.03	35.92	36	0.222
H X 7	1.5	77.42	77.4395	77.41	0.038	86.41	85.32	85	0.376

3.2.6.2. Three-fluid HX

The development of the model of the 3-fluid HX is analogous to that described above for the 2-fluid HX. The main difference lays in the fact that 3 fluids are now interested in the heat exchange process. Only the key-aspects and main difference with respect to the 2-fluids HX model are reported here.

3.2.6.2.1. Model

In **Figure 19b** the component is represented as it appears in the refrigerator model, where one cold fluid (blue, A) cools down two fluids simultaneously (orange, C and red, B). In **Figure 19c** it is shown how the 3fluidis-HX model is actually composed. This time, the single-fluid HXs from ThermoPower has been used as a base to model the three fluids. This is mainly due to the presence, as it can be appreciated in **Figure 19c**, of two thermal ports in “PipeA” (the orange parts above and below it); it takes into account the fact that fluid A is exchanging heat with two fluids at the same time. This specific component model is not present in CryoModelica. Yet again, “PipeC” is thermally connected to “PipeA” through “MetalWallAC”, which is also thermally connected to “PipeB” by the “MetalWallAB”.

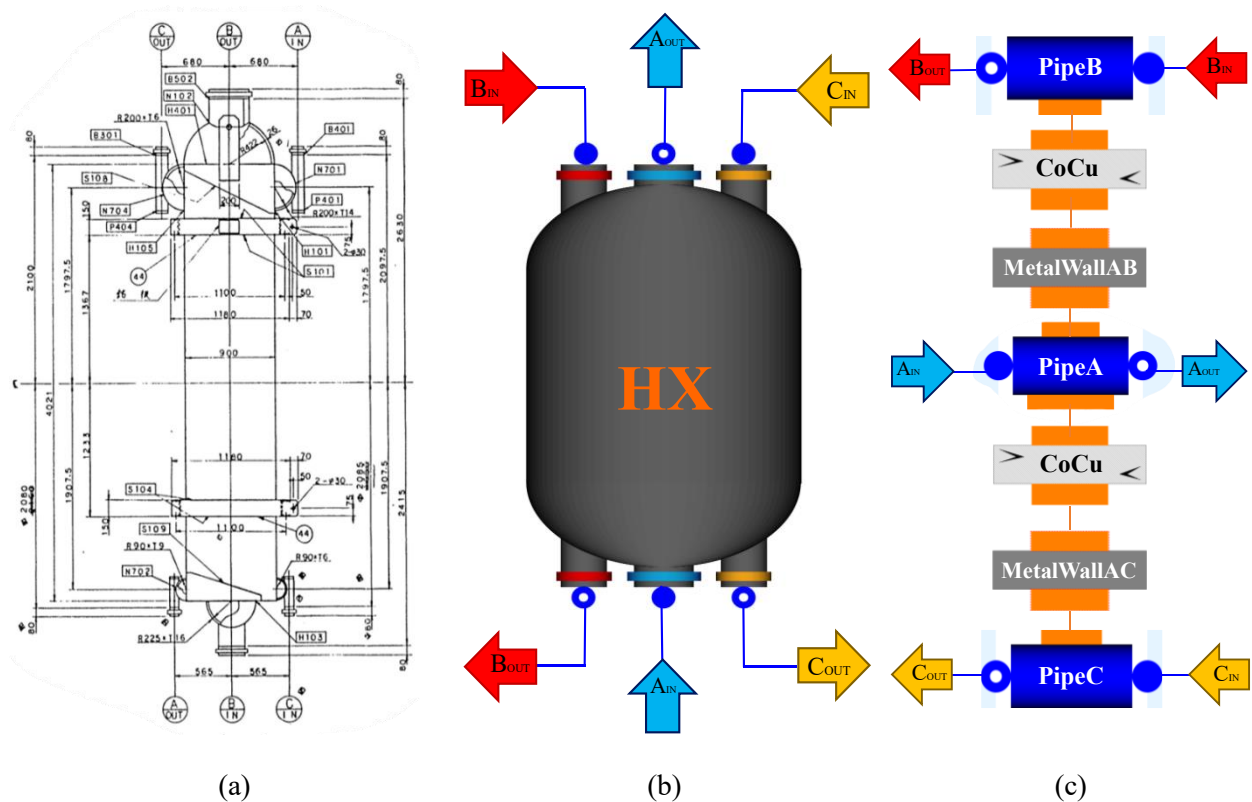


Figure 19 - (a) 3-fluid reference HX [64] (b) CryoModelica model HX (c) CryoModelica HX exploded view.

As shown in **Figure 10** and **Figure 11**, the He refrigerator is equipped with two 3-fluid HXs. The first is HX4 in which the LP He cools both the HP He streaming down from HX3 and the HP flowrate expanded in TE1. The second is HX1 in which the HP He flowing down is cooled by both the LP He and the N₂.

The model represented in **Figure 19** is fit only for one of the two 3-fluids HXs present in the refrigerator model, namely HX4. (HX1 is built with an analogous but slightly different configuration: fluid B is blue and flows bottom-up in the left-side, cooling in counterflow fluid A (red) in the middle, and this time also fluid C, namely the N₂, aids in the cooling of A, flowing bottom-up.).

Similarly to what has been said for the 2-fluids HX, in **Figure 20b** is represented the recurrence pattern of the passages as they are fit along the x-axis of the heat-exchanger. The recurrent pattern in a passage is the same of the 2-fluids HX (see **Figure 16b**).

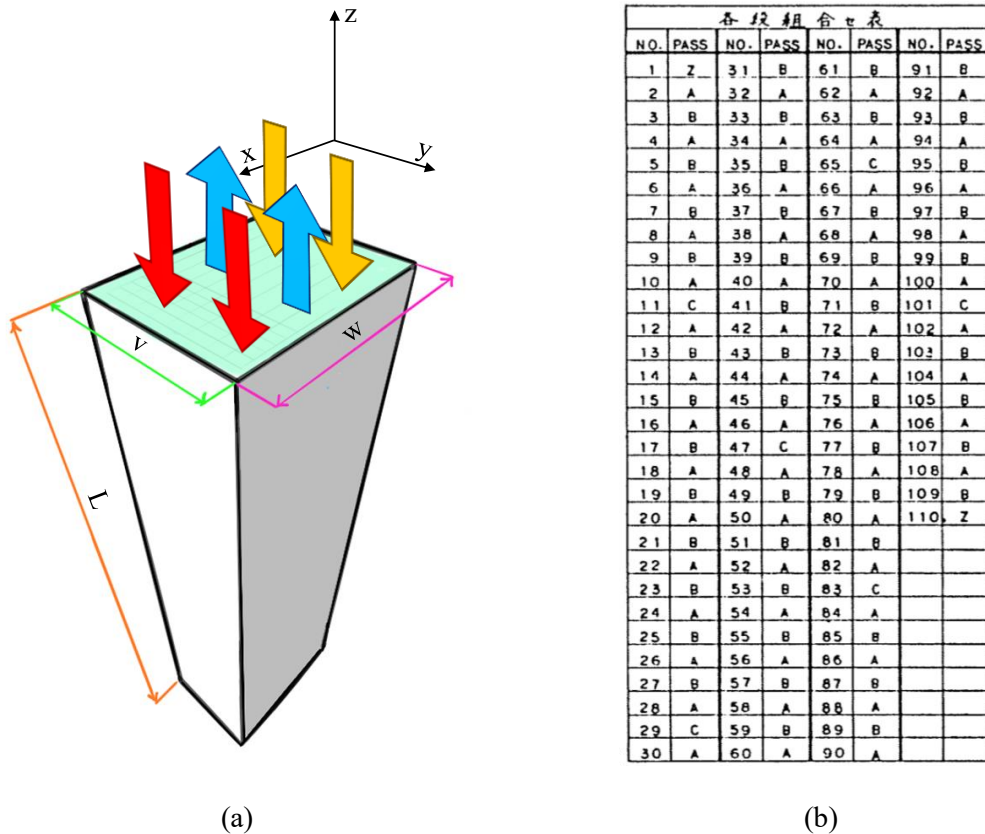


Figure 20 - (a) 3D sketch of the 3-fluid HX4. (b) Recurrence pattern of the HX: a total of 110 passages split between fluid A, B and C [64]. In this model only 108 passages are modelled, disregarding the 2 peripheral (Z) ones.

The procedure for the development of the model is completely analogous to that described in the previous section, the only difference being that instead of 2 bundles of $n_{t,A}$ and $n_{t,C}$ pipes each (and $R_{int,A}$

and $R_{int,C}$ respectively), here the upshot is 3 bundles composed by $n_{t,A}$, $n_{t,B}$, $n_{t,C}$ pipes each (and $R_{int,A}$, $R_{int,B}$ and $R_{int,C}$ respectively). Also, instead of one MetalWall here there are two of them, that will be different one from the other, since fluids A and B touch each other more frequently than fluids A and B (see **Figure 16b**).

The main results of the adopted procedure are listed in **Table 7**. To be noticed here that the height (b) of the channels are not the same for the three fluids.

Table 7 - 3-fluid HX4 data. (The same table is valid for HX1, substituting the three colour labels with Fluid Red A (warm), Fluid Blue B (cold), Fluid Green C (cold), respectively.)

		Fluid A (cold)	Fluid B (warm)	Fluid C (warm)
Real 3-fluid HX	passages	48	54	6
	b (mm)	9.50	4.70	
	c (mm)	1.40		
	δ_f (mm)	0.20		
	δ_p (mm)	1.20		
	w (mm)	847.4		
	v (mm)	864		
	L (mm)	4021		
	V_{tot} (m ³)	2.94		
	A_{tot} (m ²)	0.73		
	A_{plate} (mm ²)	1036.8		
	A_{ff} (m ²)	0.34	0.18	0.02
Model 3-fluid HX	R_{int} (mm)	8.22	3.97	3.94
	R_{ext} (mm)	8.50	4.25	4.21
	n_t	1589	3703	419

3.2.6.2.2. Tests

Also the 3-fluid HX model has been tested in normal (cold) operation to calibrate the values of β (now there are 2 of them to be set for each 3-fluid HX). Again, the comparison required for the calibration has been made with experimental measurements [64].

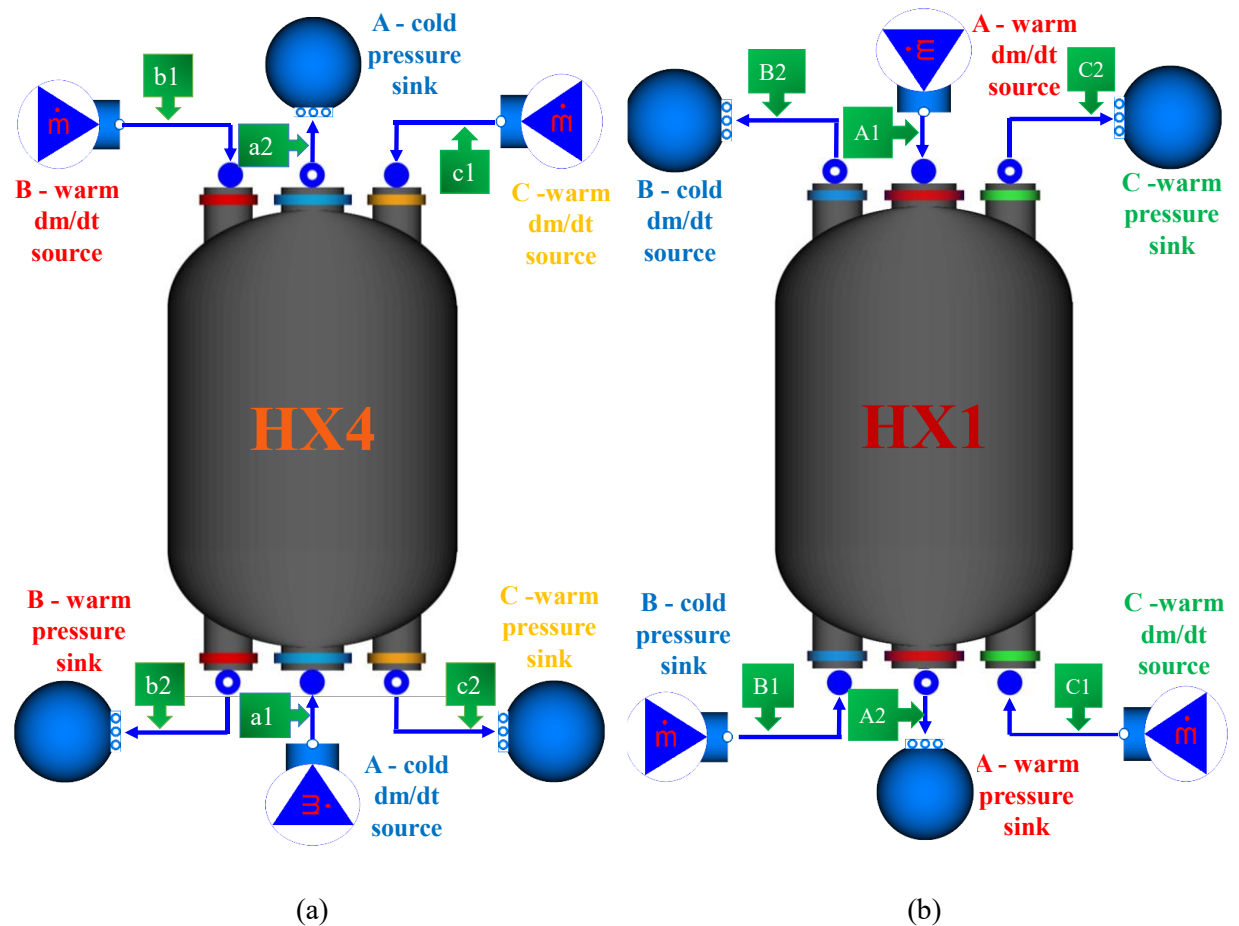


Figure 21 - 3-fluid HX model test layout. (a) HX4 test. The path of the cold cooling fluid is shown in blue. The path of the 2 warm fluids is shown in red and orange. (b) HX1 test. Notice the difference. Here fluid B is the cooling fluid, and it flows on the left, A is the warm fluid being cooled and C is the N_2 that partakes in the cooling action of B. The temperature sensors are represented in green.

The results of the tests are summarized in **Table 8**.

Table 8 - A summary of the results of the HX1 and HX4 tests is reported here. A comparison with the experimental results (coloured columns) during the calibration exercise is also provided by computing the relative difference, minimized in view of the calibration.

Result comparison 3-FLUID HX						
	β_{AB}	β_{AC}	T_{a1} [K]	T_{a2} [K]	$T_{a2,exp}$ [K]	err [%]
HX4	1.5	1.5	17.23	28.19	28.08	0.392
			T_{b1} [K]	T_{b2} [K]	$T_{b2,exp}$ [K]	err [%]
			28.59	18.65	18.6	0.269
			T_{c1} [K]	T_{c2} [K]	$T_{c2,exp}$ [K]	err [%]
			28.59	17.84	18.6	4.086
	β_{AB}	β_{AC}	T_{A1} [K]	T_{A2} [K]	$T_{A2,exp}$ [K]	err [%]
HX1	1.47	0.0018	313	86.6	86.41	0.220
			T_{B1} [K]	T_{B1} [K]	$T_{B1,exp}$ [K]	err [%]
			83.52	305.4	308	0.844
			T_{C1} [K]	T_{C2} [K]	$T_{C1,exp}$ [K]	err [%]
			77.44	275.4	273	0.879

4. Simulation setup

Since the aim here is not to validate the refrigerator model, but to assess its capabilities to work in dynamic conditions, the simulations described here are used to proof these capabilities not referred necessarily to any real transient, as the implementation of the detailed controls would be required. The simulations are then targeted at showing that when some perturbation is introduced (progressive closure of a valve, variation of the rpm of the CC or pulsed heat load to the HeBath, closer to the real operation of such a refrigerator), all the system is perturbed, and the model responds coherently.

The simulation has been performed by integrating with the DASSL algorithm (a differential/algebraic system solver) [68], with a tolerance of $1e-7$ and an adaptive refinement of the time-step.

4.1. Pulsed heat source

The first transient that is shown here (see **Figure 22**), is a periodic pulsed heat deposition on the HeBath. Every 3600 s a pulse of 2000 W is fed to the HeBath.

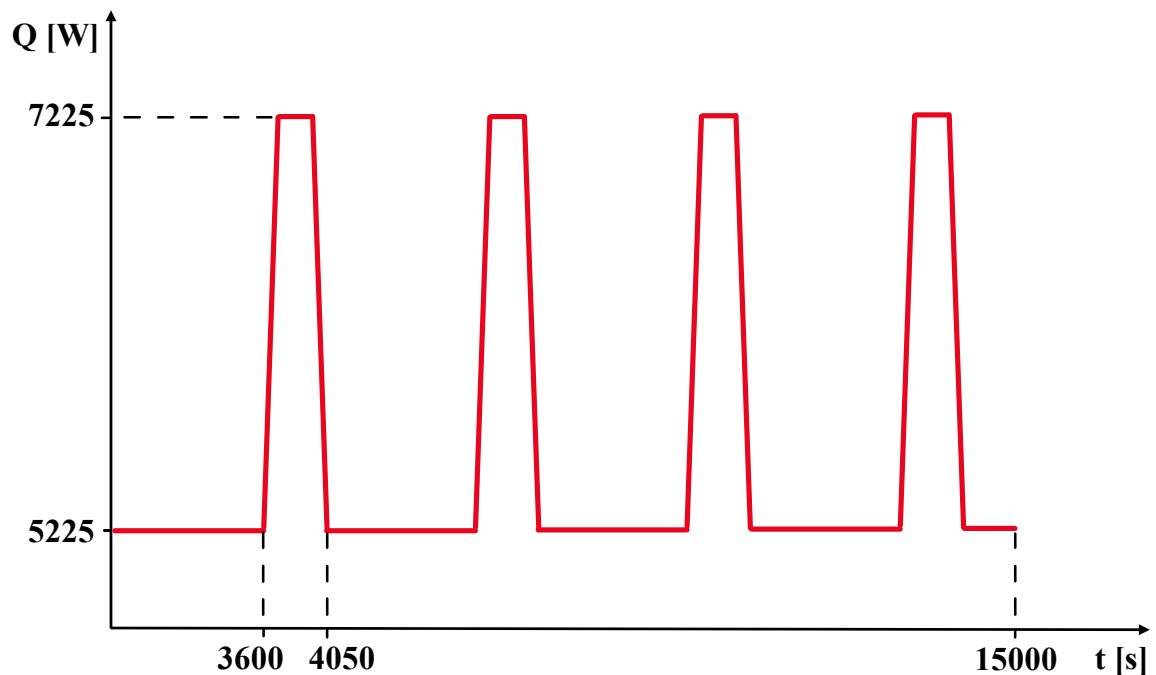


Figure 22 - Trapezoidal heat pulse source fed to the LHe bath in the refrigerator model. Period = 3600s; rise = 150s; amplitude = 2000 W; offset = 5225 W; start time = 3600 s.

4.2. Progressive closure of JT3

The second transient still features the same pulsed heat deposition described above, but with an additional perturbation of the system. JT3 is progressively closed (see **Figure 23**).

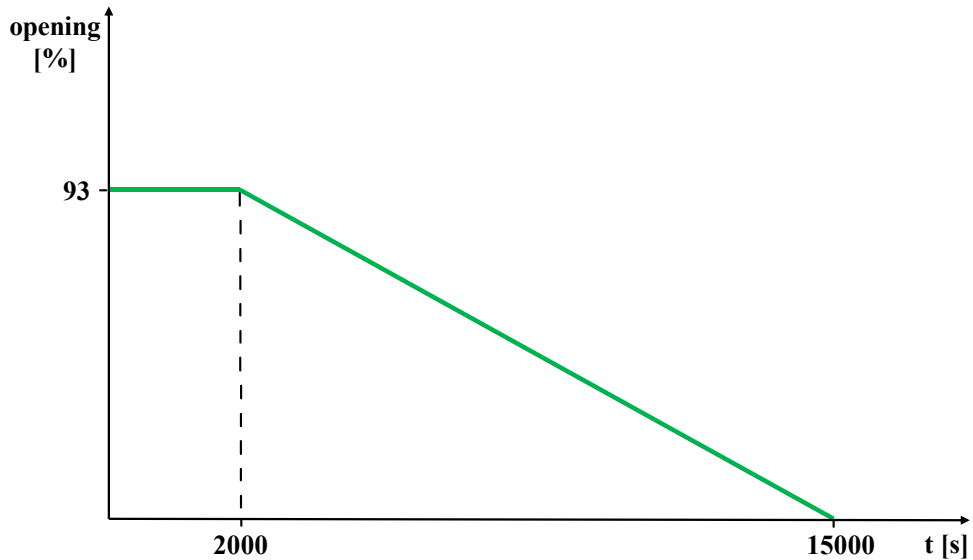


Figure 23 - JT3 progressive closure. Offset = 93 %; start time = 2000 s.

4.3. CC partial LOFA

The third transient is again the same pulsed heat deposition described above, but this time featuring also a partial loss of flow accident (LOFA) in the CC. The rpm of the CC which has been kept fixed so far, is exponentially halved (see **Figure 24**).

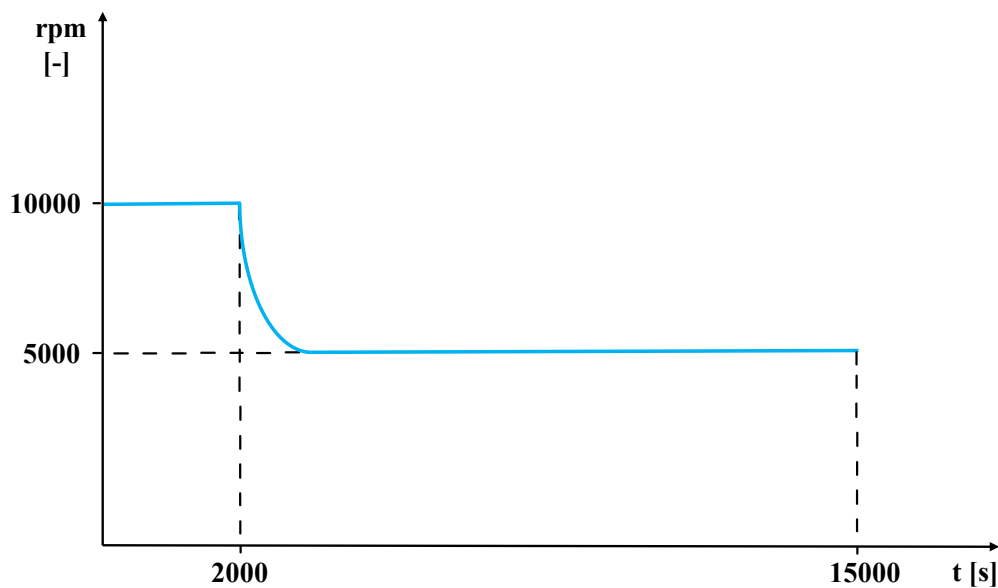


Figure 24 - CC Partial LOFA. Start Time = 2000s; offset = 10000 rpm; final value = 5000 rpm.

5. Results

In this section the results for the three simulations described above are reported. It is expected a variation of the trend of the physical parameters describing the circuit, i.e., the liquid level within the HeBath, the operating point of the CC, the pressure, temperature, and mass flow rate along the circuit. Some interesting spots have been selected along the circuit to show how the refrigerator model reacts to different types of perturbations. Sensors have been positioned there and the readings are presented here below. See **Figure 10** and **Figure 11** for location of the sensors and components along the circuit.

In **Figure 25** the PS1 reading for the three transients is shown. In the yellow circles (see **Figure 25**) can be appreciated the effect of the heat pulse on the fluid pressure. The closure of JT3 produced quite a drastic increase of pressure (red line in **Figure 25**): closing JT3, the mass flowrate along the red line (see **Figure 10** and **Figure 11**) started to increase (see red line in **Figure 25**), leading to an overfilling of the HeBath (see **Figure 27**). Conversely, the LOFA on top of the heat pulses, made the liquid level of the HeBath decrease (and its pressure) with an ever-steeper slope, leading to an interruption of the simulation to avoid the emptying of the bath. The reason for this liquid draining can be appreciated in **Figure 26**. The reduction of the rpm of the CC, lead to a shifting of the OP, that made the mass flowrate increase. Thus, the CC started sucking out of the bath more than what entered, the liquid drained, and the pressure decreased.

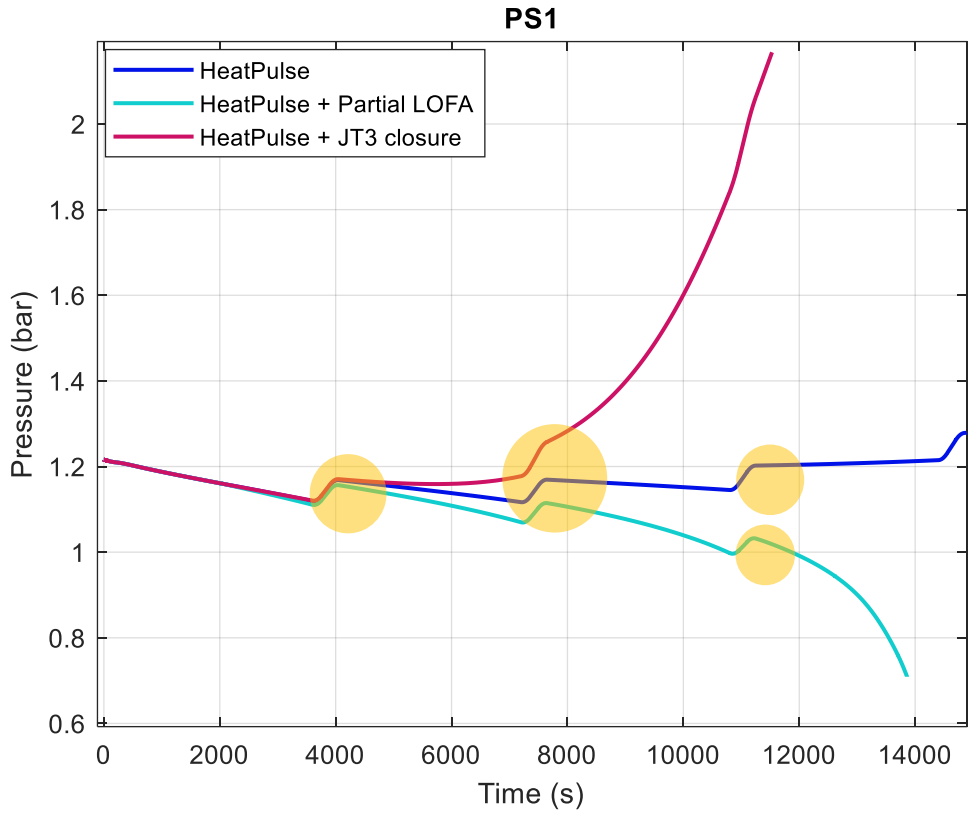


Figure 25 - PS1 reading. CC inlet pressure.

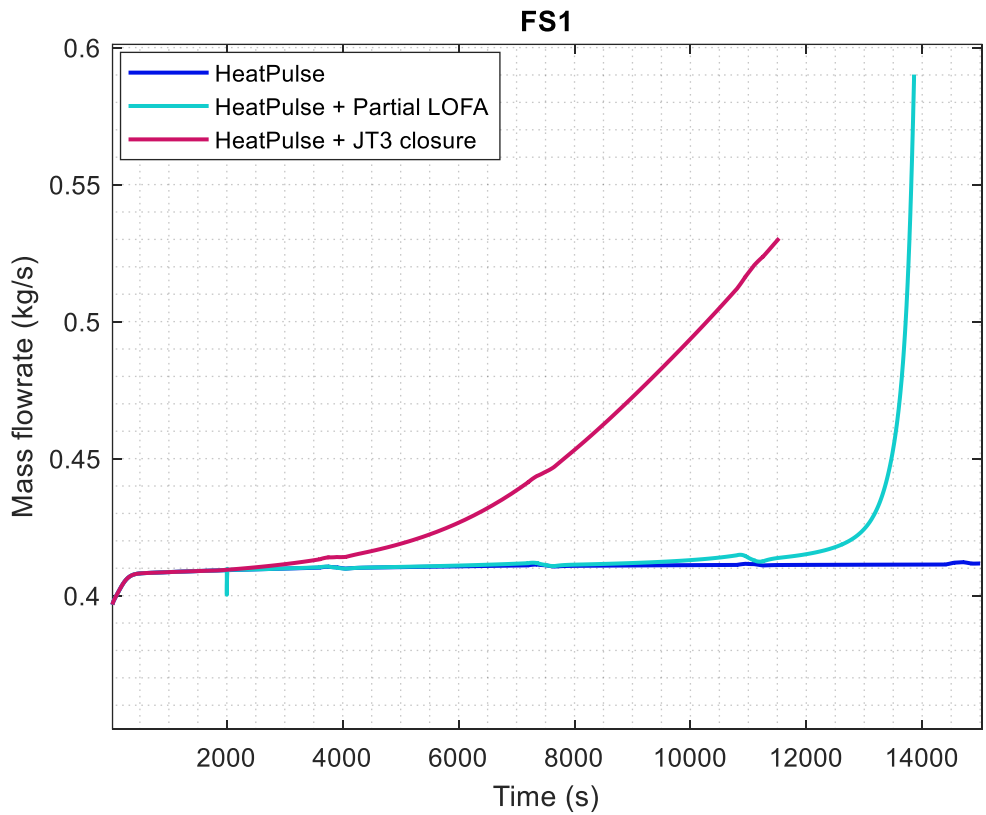


Figure 26 - FS1 reading. CC mass flowrate.

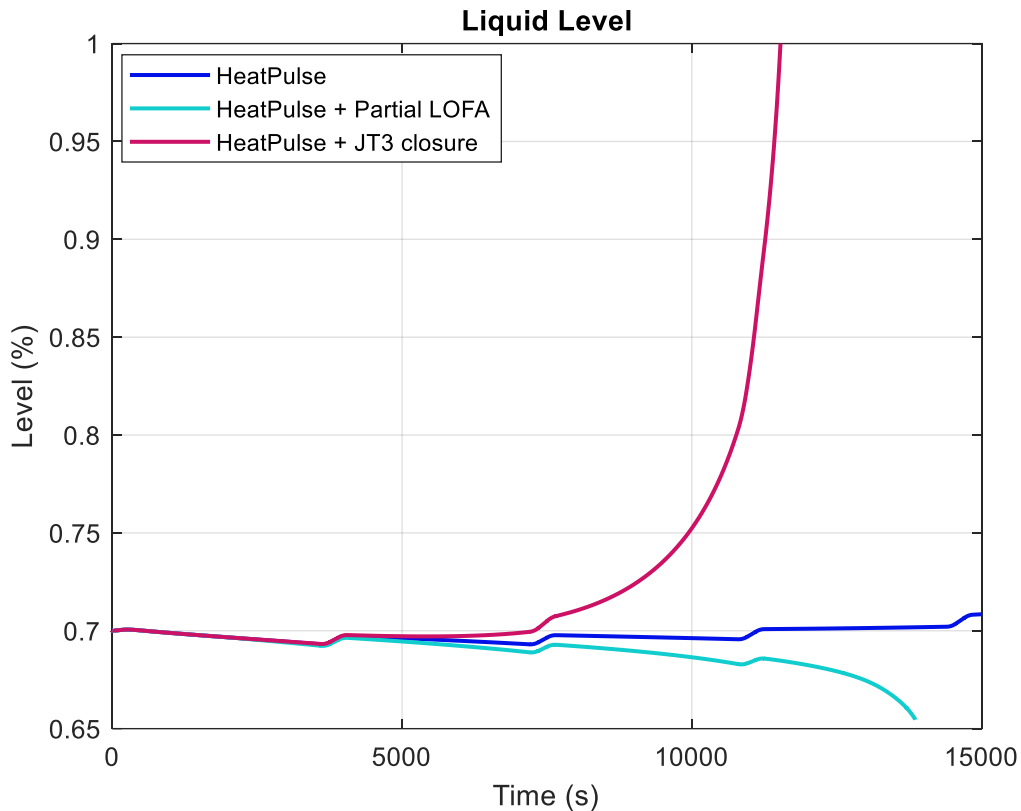


Figure 27 - Liquid Level of the HeBath.

As expected, also the mass flowrate along the circuit, and in particular the one passing through JT3 (see **Figure 28**) and the PR of the turbines, e.g., TE2 (see **Figure 29**) are influenced by the closing of JT3 and the partial LOFA: as the mass flowrate increases the PR increases (and vice-versa).

In **Figure 30** and **Figure 31** is shown how also temperatures and pressures along the circuits were affected by the different transients. Both experienced the greatest modification in the third transient, when closing JT3; as expected, the temperature increased (see **Figure 31**). This is due to the closing of the turbines line, which plays a key role in the cooling stage (He is greatly cooled there before reaching the client). Lacking the coolant of the isentropic expansions, T globally increases. And this temperature increase causes a considerable increase of pressure too (**Figure 30**) in the same time-scales. This is because the circuit is isochoric, thus an increase of the global He temperature produces a swift increase of its pressure as well.

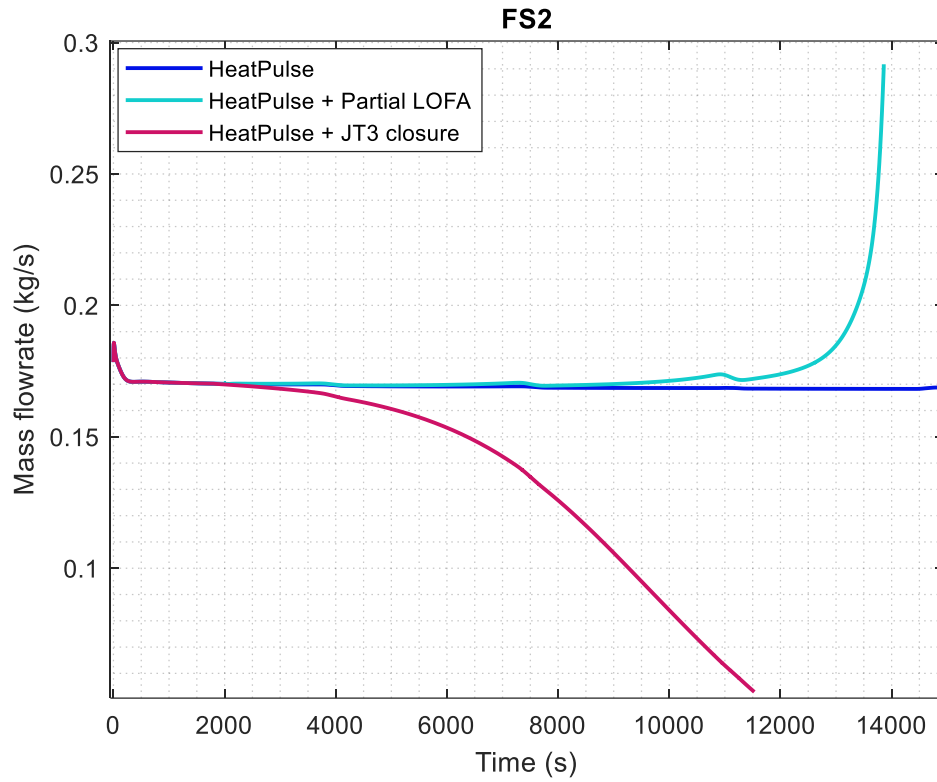


Figure 28 – Mass flowrate along JT3 for the three transients.

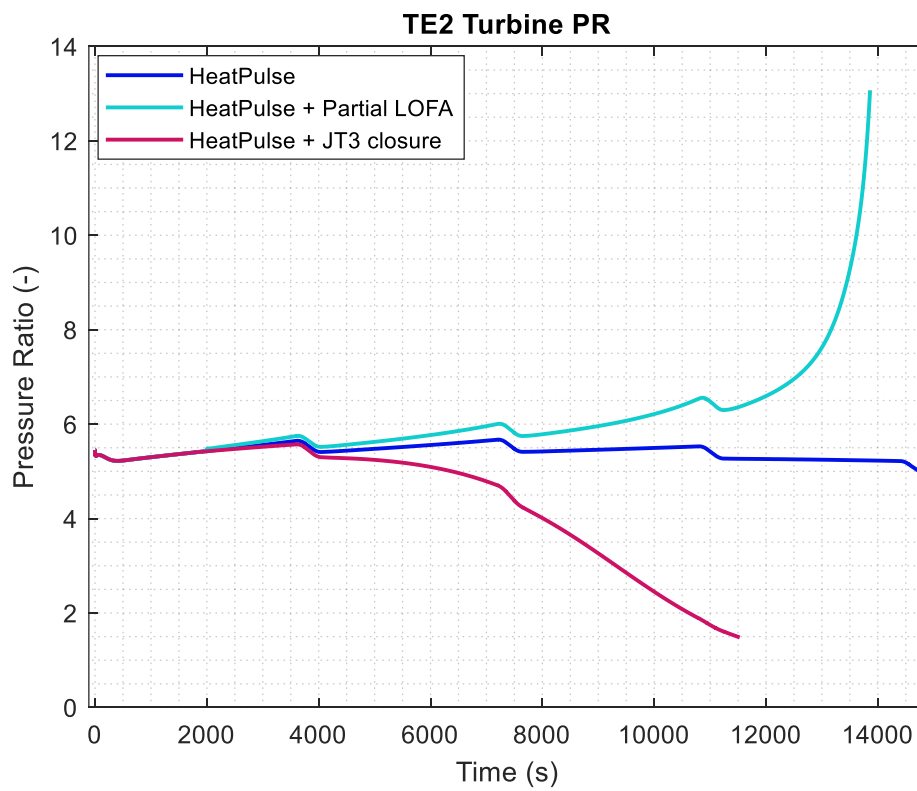


Figure 29 – PR modification of TE2 for the three transients.

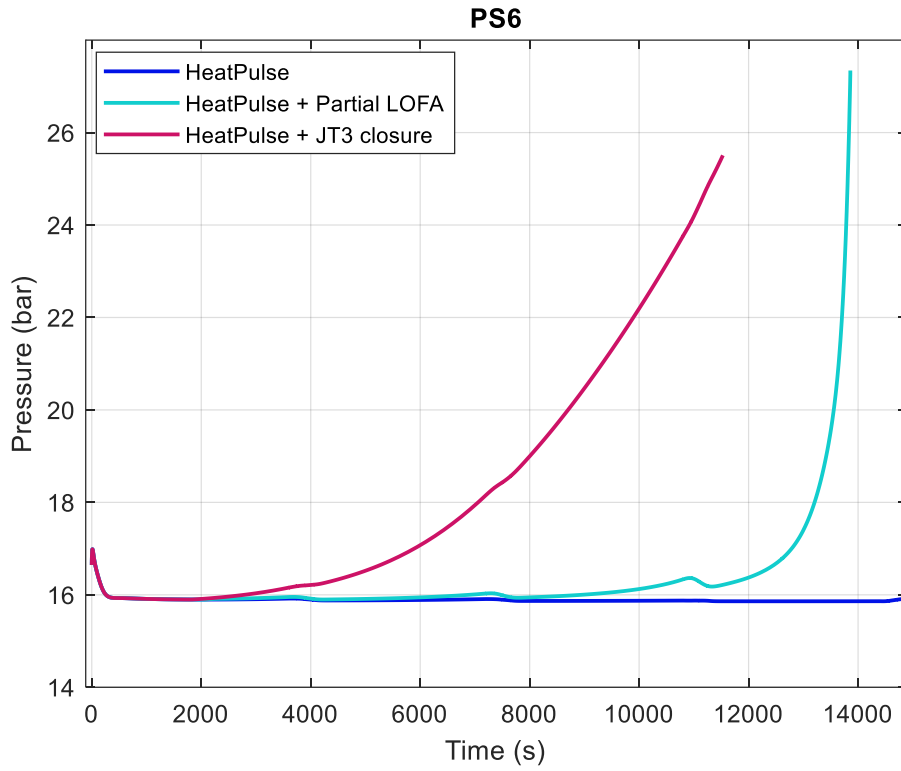


Figure 30 - Pressure modification in two different points of the circuits for the three transients.

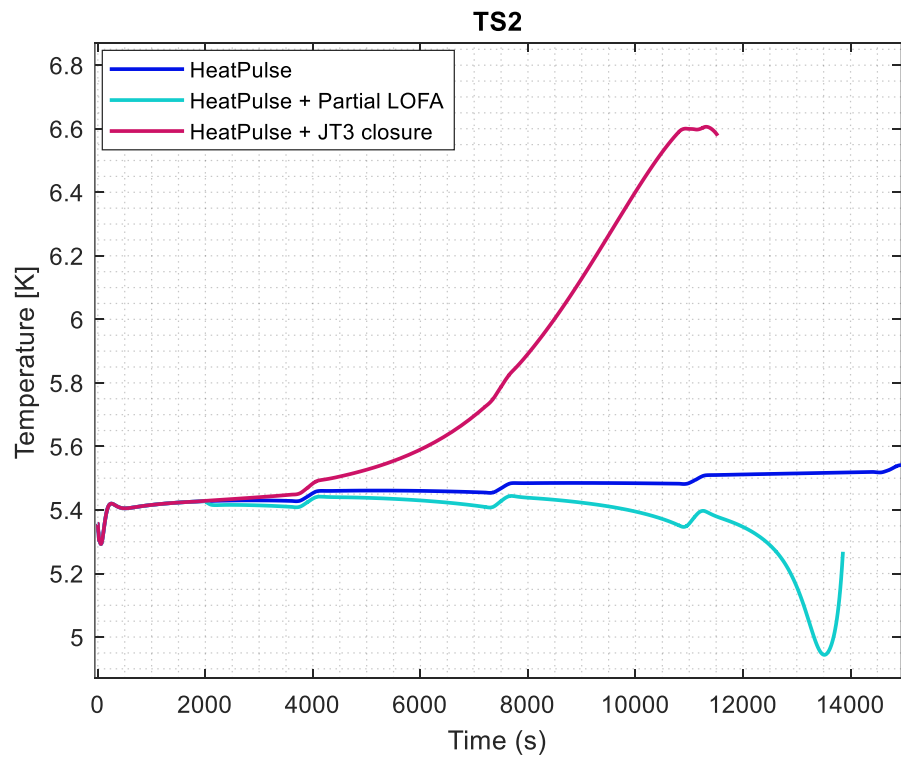


Figure 31 - TS2 temperature reading.

6. Conclusions and perspectives

The aim of the present work was the development of a dynamic model for the CSMC Naka refrigerator, whose structure and operation is very similar to other existing refrigerators for nuclear fusion applications. Although other refrigerator models have already been designed, they are either too computationally expensive, or partial (including only a part of the refrigerator) or steady-state. The Modelica programming language has been chosen to complete this task.

Base components from already available libraries (ThermoPower and CryoModelica) have been used to build the model, or to assemble new complex dynamic components as the two-fluid and three-fluid HXs. Each component has been tested and (whenever needed) suitably calibrated, before being included in the full model of the refrigerator. The latter includes the entire thermodynamic Collins loop: the warm (multi-stage) compressor, the nitrogen pre-cooling, the cooling stage (featuring the isentropic expansion in the turbines) and the post-cooling with the Joule-Thompson isenthalpic expansion stages.

Although this refrigerator model does not include all the controllers (for which there are only partially available information), it has been applied to the preliminary and demonstrative analysis of some relevant transients relevant for the operating conditions of a pulsed coil. The results proved to be realistic and consistent with the expectations.

This first model represents an important milestone in the modelling of the cryoplant for one of the most expensive systems of a tokamak, being pursued together with the modelling of the superconducting magnet system to try and set-up proper automatic control strategies for the operation of such complex objects in future reactors.

For this reason, as a next step, the implementation of automatic controllers is foreseen, e.g., for the cold compressor rpm and for the valves opening. Moreover, the simulation of a complex transient as the magnet cooldown is also envisaged. This will also allow to validate the model against the data available from the CSMC tests.

Bibliography

- [1] H. Ritchie, “Energy Mix.” <https://ourworldindata.org/energy-mix> (accessed Mar. 10, 2021).
- [2] D. Kramer, “Investments in privately funded fusion ventures grow,” *Phys. Today*, vol. 2020, no. 2, p. 1013a, Oct. 2020, doi: 10.1063/pt.6.2.20201013a.
- [3] EUROfusion, “History of Fusion.” <https://www.euro-fusion.org/fusion/history-of-fusion/> (accessed Mar. 08, 2021).
- [4] D. Geere, “Cern breaks man-made heat record with ~5.5 trillion degree plasma,” *WIRED*, Aug. 2012.
- [5] R. H. Majeed and O. N. Oudah, “Reaching to a featured formula to deduce the energy of the heaviest particles producing from the controlled thermonuclear fusion reactions,” *J. Phys. Conf. Ser.*, vol. 1003, no. 1, 2018, doi: 10.1088/1742-6596/1003/1/012076.
- [6] E. I. Moses, “The National Ignition Facility (NIF): A path to fusion energy,” *Energy Convers. Manag.*, vol. 49, no. 7, pp. 1795–1802, 2008, doi: 10.1016/j.enconman.2007.10.029.
- [7] R. C. Kirkpatrick, “Magnetized target fusion-an overview,” in *International Conference on Plasma Sciences (ICOPS)*, Jun. 1993, pp. 105-, doi: 10.1109/PLASMA.1993.593107.
- [8] P. H. Rebut, “ITER: the first experimental fusion reactor,” *Fusion Eng. Des.*, vol. 27, no. C, pp. 3–16, 1995, doi: 10.1016/0920-3796(95)90113-2.
- [9] P. (<https://physics.stackexchange.com/users/156112/physicsphun>), “How many times does plasma do a full loop tokamak before fusion?” [Online]. Available: <https://physics.stackexchange.com/q/333151>.
- [10] D. Clery, “Twisted logic,” *Science (80-.)*, vol. 350, no. 6259, pp. 369–371, 2015, doi: 10.1126/science.350.6259.369.
- [11] Subkect Zero Science, “Stellarators - The Future of Fusion Energy [2020],” 2020. <https://www.youtube.com/watch?v=qKTePWmHRQw> (accessed Mar. 10, 2020).
- [12] Y. Xu, “A general comparison between tokamak and stellarator plasmas,” *Matter Radiat. Extrem.*, vol. 1, no. 4, pp. 192–200, 2016, doi: 10.1016/j.mre.2016.07.001.
- [13] G. McCracken and P. Stott, “Man-Made Fusion,” in *Fusion*, Elsevier, 2005, pp. 33–46.
- [14] The Editors of Encyclopaedia, “Tritium,” *Encyclopedia Britannica*. 2018, [Online]. Available: <https://www.britannica.com/science/tritium>.
- [15] R. J. Pearson, A. B. Antoniazzi, and W. J. Nuttall, “Tritium supply and use: a key issue for the development of nuclear fusion energy,” *Fusion Eng. Des.*, vol. 136, pp. 1140–1148, Nov. 2018,

doi: 10.1016/j.fusengdes.2018.04.090.

- [16] C. Day, “Seminar in the framework of the Nuclear Fusion Engineering course at Politecnico di Torino.” 2020.
- [17] EUROfusion, “The demonstration power plant: DEMO.” <https://www.eurofusion.org/programme/demo/> (accessed Mar. 08, 2021).
- [18] R. Arnoux, “SUPERCONDUCTIVITY: IT GETS THE CURRENT FLOWING - ITER MAG 5,” 2014. <https://www.iter.org/mag/5/40w> (accessed Mar. 08, 2021).
- [19] D. M. Ginsberg, “Superconductivity,” *Encyclopedia Britannica*. 2018, [Online]. Available: <https://www.britannica.com/science/superconductivity>.
- [20] FUSION FOR ENERGY, “ITER The Device.” <https://fusionforenergy.europa.eu/the-device/> (accessed Mar. 11, 2021).
- [21] J. G. Bednorz and K. A. Müller, “Possible highTc superconductivity in the Ba–La–Cu–O system,” *Zeitschrift für Phys. B Condens. Matter*, vol. 64, no. 2, pp. 189–193, 1986, doi: 10.1007/BF01303701.
- [22] M. P. Paranthaman and T. Izumi, “High-Performance Superconductor Wires,” no. August 2004, pp. 533–541, 2021.
- [23] M. Noe, R. Heller, W. Fietz, W. Goldacker, T. Schneider, and F. Karlsruhe, “HTS applications,” *Proc. - Work. Accel. Magn. Supercond. Des. Optim. WAMSDO 2008*, Jan. 2009.
- [24] J. Emanuelson and S. Pike, “RESISTANCE vs. TEMPERATURE & PERSISTENT CURRENT IN A RING.” 1998, [Online]. Available: <http://www.futurescience.com/manual/sc1000.html>.
- [25] R. Zanino and L. Savoldi Richard, “A review of thermal-hydraulic issues in ITER cable-in-conduit conductors,” *Cryogenics (Guildf)*., vol. 46, no. 7–8, pp. 541–555, Jul. 2006, doi: 10.1016/j.cryogenics.2006.01.007.
- [26] L. Savoldi Richard, F. Casella, B. Fiori, and R. Zanino, “The 4C code for the cryogenic circuit conductor and coil modeling in ITER,” *Cryogenics (Guildf)*., vol. 50, no. 3, pp. 167–176, Mar. 2010, doi: 10.1016/j.cryogenics.2009.07.008.
- [27] R. Zanino, R. Bonifetto, C. Hoa, and L. Savoldi, “Verification of the Predictive Capabilities of the 4C Code Cryogenic Circuit Model,” *Adv Cryo Eng AIP Conf Proc*, vol. 1573, 2013, doi: 10.1063/1.4860896.
- [28] R. Zanino, R. Bonifetto, A. Brighenti, T. Isono, H. Ozeki, and L. Savoldi, “Prediction, experimental results and analysis of the ITER TF insert coil quench propagation tests, using the 4C code,” *Supercond. Sci. Technol.*, vol. 31, no. 3, p. 035004, Jul. 2018, doi: 10.1088/1361-

6668/aa9e6c.

- [29] R. Zanino, R. Bonifetto, R. Heller, and L. Savoldi Richard, "Validation of the 4C Thermal-Hydraulic Code Against 25 kA Safety Discharge in the ITER Toroidal Field Model Coil (TFMC)," *IEEE Trans. Appl. Supercond.*, vol. 21, no. 3, pp. 1948–1952, Jun. 2011, doi: 10.1109/TASC.2010.2089771.
- [30] R. Bonifetto, A. Kholia, B. Renard, K. Riße, L. S. Richard, and R. Zanino, "Modeling of W7-X superconducting coil cool-down using the 4C code," in *Fusion Engineering and Design*, Oct. 2011, vol. 86, no. 6–8, pp. 1549–1552, doi: 10.1016/j.fusengdes.2010.12.070.
- [31] R. Zanino, R. Bonifetto, L. S. Richard, and F. Casella, "Dynamic modeling of a supercritical helium closed loop with the 4C code," vol. 1434, p. 1743, 2012, doi: 10.1063/1.4707109.
- [32] R. Bonifetto *et al.*, "Analysis of the cooldown of the ITER central solenoid model coil and insert coil," *Supercond. Sci. Technol.*, vol. 30, no. 1, p. 015015, Jan. 2017, doi: 10.1088/0953-2048/30/1/015015.
- [33] R. Bonifetto, A. Brighenti, L. Savoldi, and R. Zanino, "Coupling superconducting magnet and refrigerator thermal-hydraulic models for nuclear fusion applications," *IOP Conf. Ser. Mater. Sci. Eng.*, vol. 502, no. 1, 2019, doi: 10.1088/1757-899X/502/1/012130.
- [34] L. Savoldi Richard, R. Bonifetto, A. Foussat, N. Mitchell, K. Seo, and R. Zanino, "Mitigation of the Temperature Margin Reduction due to the Nuclear Radiation on the ITER TF Coils," *IEEE Trans. Appl. Supercond.*, vol. 23, no. 3, p. 4201305, Jun. 2013, doi: 10.1109/TASC.2013.2238977.
- [35] R. Bonifetto *et al.*, "Computation of JT-60SA TF coil temperature margin using the 4C code," in *Fusion Engineering and Design*, Oct. 2011, vol. 86, no. 6–8, pp. 1493–1496, doi: 10.1016/j.fusengdes.2011.02.068.
- [36] R. Zanino, R. Bonifetto, C. Hoa, and L. Savoldi Richard, "4C modeling of pulsed-load smoothing in the HELIOS facility using a controlled bypass valve," *Cryogenics (Guildf.)*, vol. 57, pp. 31–44, Oct. 2013, doi: 10.1016/j.cryogenics.2013.04.005.
- [37] F. Guelfi, R. Bonifetto, C. Hoa, L. Savoldi, and R. Zanino, "4C modeling of the supercritical helium loop HELIOS in isobaric configuration," *Cryogenics (Guildf.)*, vol. 64, pp. 51–62, Nov. 2014, doi: 10.1016/j.cryogenics.2014.09.003.
- [38] C. Hoa *et al.*, "HELIOS helium loop for high loads smoothing: a cryogenic scaled down experiment of the cooling circuit of JT-60SA superconducting magnets," 2010.
- [39] R. Maekawa, K. Ooba, M. Nobutoki, and T. Mito, "Dynamic simulation of the helium

- refrigerator/liquefier for LHD,” *Cryogenics (Guildf)*., vol. 45, no. 3, pp. 199–211, Mar. 2005, doi: 10.1016/j.cryogenics.2004.10.001.
- [40] B. Bradu, P. Gayet, and S. I. Niculescu, “A process and control simulator for large scale cryogenic plants,” *Control Eng. Pract.*, vol. 17, no. 12, pp. 1388–1397, Dec. 2009, doi: 10.1016/j.conengprac.2009.07.003.
- [41] C. Deschildre *et al.*, “DYNAMIC SIMULATION OF AN HELIUM REFRIGERATOR,” *AIP Conf. Proc.*, vol. 985, p. 949, 2008, doi: 10.1063/1.2908587.
- [42] N. Peng, L. Xiong, L. Liu, L. Serio, and L. Zhang, “Thermo-hydraulic analysis of cooldown for ITER toroidal field coils from 80 K to 6 K,” vol. 1434, p. 1706, 2012, doi: 10.1063/1.4707104.
- [43] W. Abdel Maksoud *et al.*, “Commissioning of the Cold Test Facility for the JT-60SA Tokamak Toroidal Field Coils,” *IEEE Trans. Appl. Supercond.*, vol. 26, no. 4, pp. 1–6, Jun. 2016, doi: 10.1109/TASC.2015.2510225.
- [44] Y. Wu, H. Liu, Y. Shi, J. Chen, and Z. Ren, “The cryogenic system for ITER CC superconducting conductor test facility,” *Cryogenics (Guildf)*., vol. 51, pp. 62–67, 2011, doi: 10.1016/j.cryogenics.2010.11.004.
- [45] B. Sarkar *et al.*, “1 kW Class He Refrigerator/Liquefier for SST-1,” in *Proceedings of 18th International Cryogenics Engineering Conference*, 2000, pp. 123–126.
- [46] R. Garbil *et al.*, “The Tore Supra Cryoplant control system upgrade,” *Fusion Eng. Des.*, vol. 58–59, pp. 217–223, Nov. 2001, doi: [https://doi.org/10.1016/S0920-3796\(01\)00437-9](https://doi.org/10.1016/S0920-3796(01)00437-9).
- [47] K. Schaubel, A. Langhorn, S. Lloyd, Z. Piec, E. Salazar, and J. Smith, “The ITER Central Solenoid Module final test facility,” *Fusion Eng. Des.*, vol. 124, pp. 59–63, Nov. 2017, doi: 10.1016/j.fusengdes.2017.05.010.
- [48] H. Bai *et al.*, “Cryogenics in EAST,” *Fusion Eng. Des.*, vol. 81, no. 23, pp. 2597–2603, 2006, doi: <https://doi.org/10.1016/j.fusengdes.2006.07.048>.
- [49] K. Hamada *et al.*, “Final design of a cryogenic system for the ITER CS model coil,” *Cryogenics (Guildf)*., vol. 34, no. SUPPL. 1, pp. 65–68, Jan. 1994, doi: 10.1016/S0011-2275(05)80011-6.
- [50] Y. Bozhko and F. Schauer, “Refrigeration system for W7-X,” *Nucl. Fusion*, vol. 43, no. 9, pp. 835–841, Sep. 2003, doi: 10.1088/0029-5515/43/9/307.
- [51] K. Yoshida *et al.*, “Cryogenic system for JT-60SA Specialization of the cryogenic system for superconducting magnets of a tokamak device,” *Teion Kogaku*, vol. 50, no. 12, pp. 575–582, 2015, [Online]. Available: http://inis.iaea.org/search/search.aspx?orig_q=RN:47080026.
- [52] C. H. Choi *et al.*, “Helium refrigeration system for the KSTAR,” *Fusion Eng. Des.*, vol. 81, no.

- 23–24, pp. 2623–2631, Nov. 2006, doi: 10.1016/j.fusengdes.2006.07.019.
- [53] “ITER website.” <http://www.iter.org> (accessed Mar. 09, 2021).
- [54] S. E. Mattsson, H. Elmqvist, and M. Otter, “Physical system modeling with Modelica,” in *Control Engineering Practice*, Apr. 1998, vol. 6, no. 4, pp. 501–510, doi: 10.1016/S0967-0661(98)00047-1.
- [55] F. Casella and A. Leva, “Modelica open library for power plant simulation: design and experimental validation,” in *Proceedings of the 3rd International Modelica Conference*, 2003, pp. 41–50, [Online]. Available: <http://scholar.google.com/scholar?hl=en&btnG=Search&q=intitle:Modelica+open+library+for+power+plant+simulation+:+design+and+experimental+validation#0>.
- [56] “Modelica Standard Library, Version 3.2.2.” <https://github.com/modelica/ModelicaStandardLibrary> (accessed Mar. 10, 2021).
- [57] E. W. Lemmon, M. L. Huber, M. O. McLinden, and I. Bell, “Reference Fluid Thermodynamic and Transport Properties.” NIST Standard Reference Database 23, Version 9.1, 2013.
- [58] F. Casella and C. Richter, “ExternalMedia: a Library for Easy Re-Use of External Fluid Property Code in Modelica,” pp. 157–161, 2008, Accessed: Mar. 10, 2021. [Online]. Available: <https://re.public.polimi.it/handle/11311/550476#.YEjfxNWcReU.mendeley>.
- [59] H. Tsuji *et al.*, “Progress of the ITER central solenoid model coil programme,” *Nucl. Fusion*, vol. 41, no. 5, pp. 645–651, May 2001, doi: 10.1088/0029-5515/41/5/319.
- [60] A. R. Jha, “Cryogenic Technology and Applications,” *Cryog. Technol. Appl.*, Jan. 2006, doi: 10.1016/B978-0-7506-7887-2.X5000-X.
- [61] ITER Design Description Document, “TF Coils and Structures.” ITER_D_2MVZNX v2.2, 2009.
- [62] B. Lagier, C. Hoa, and B. Rousset, “Dynamic modelling of a forced flow supercritical helium loop with EcosimPro,” in *ICEC 24 - ICMC 2012: Proceedings of 24th international cryogenic engineering conference and international cryogenic materials conference 2012*, 2012, p. 932, [Online]. Available: http://inis.iaea.org/search/search.aspx?orig_q=RN:46064450.
- [63] R. Vallcorba, D. Hitz, B. Rousset, B. Lagier, and C. Hoa, “Investigations of pulsed heat loads on a forced flow supercritical helium loop: Part B: Simulation of the cryogenic circuit,” *Cryogenics (Guildf.)*, vol. 52, no. 7–9, pp. 349–361, Jul. 2012, doi: 10.1016/j.cryogenics.2012.02.005.
- [64] K. Kawano, “CB30_Ex_Data, personal communication.” 2015.
- [65] T. Kato, K. Hamada, K. Kawano, and T. Hiyama, *Cryogenic system for ITER CS model coil*. United States: Plenum Press, 1996.

- [66] K. Kawano, “5kw-refrigerator equipment_R, personal communication.” 2015.
- [67] K. Guo, N. Zhang, and R. Smith, “Optimisation of fin selection and thermal design of counter-current plate-fin heat exchangers,” *Appl. Therm. Eng.*, vol. 78, pp. 491–499, Mar. 2015, doi: 10.1016/j.applthermaleng.2014.11.071.
- [68] L. R. Petzold, “A DifferentiaVAgebraic System Solver,” vol. 94550, 1982.